Comparative pushover and limit analyses on seven masonry churches damaged by the 2012 Emilia-Romagna (Italy) seismic events: Possibilities of non-linear finite elements compared with pre-assigned failure mechanisms

Gabriele Milani *, Marco Valente

Department of Architecture, Built Environment & Construction Engineering ABC, Politecnico di Milano, Piazza Leonardo da Vinci 32, 20133 Milan, Italy

Received 9 June 2014
Received in revised form 22 September 2014
Accepted 29 September 2014
Available online 22 October 2014

1. Introduction

The evaluation of the seismic vulnerability of historical masonry monumental buildings [1–4] in general, and of masonry churches in particular [5–14], is a fundamental task in highly civilized countries.

This concept is especially applicable for Italy, which hosts the largest amount of monumental churches in the world and where some earthquakes, occurred in the last few decades (Umbria-Marche 1997–1998, Abruzzo 2009, Emilia-Romagna 2012), severely damaged a number of unique pieces of the architectural heritage.

* Corresponding author. Tel.: +39 022399 4290; fax: +39 022399 4220.
E-mail address: gabriele.milani@polimi.it (G. Milani).

The paper focuses on the analysis of seven masonry churches that suffered damage during the last Emilia-Romagna (2012) seismic event. The devastating 5.9 and 5.8 magnitude shakes, occurred in the north-east region of Italy called Emilia-Romagna respectively on the 20th and 29th of May 2012, caused 28 victims and several collapses of precast concrete and masonry structures [15–17].

It has been recently calculated that, only in the provinces of Modena, Ferrara and Bologna, the churches considered unsafe after the seismic sequence are more than 500.

Generally, all existing masonry structures are rather vulnerable to earthquakes, but churches in particular are not conceived to properly withstand horizontal loads. It is well known, indeed, that churches exhibit partial collapses at very low levels of horizontal acceleration. The reasons justifying such a high vulnerability are in very specific architectonical features, i.e. high and slender perimeter walls scarcely interconnected, long and wide naves carried by slender columns, quite poor masonry quality and presence of flexible wooden roofs [3–14].

The post-earthquake problems still open are (1) to evaluate the most suitable strategy of rehabilitation, limiting times and costs, and (2) to have a quantitative information on the residual resistance for the un-collapsed structures [18–20].

Both previous tasks are rather specific and hard to be tackled, because churches cannot be reduced to any standard static scheme. At present, the most diffused approach adopted in practice, as recommended by Italian Guidelines for the Cultural Heritage [21], is the utilization of the kinematic theorem of limit analysis for no-tension materials, with pre-assigned partial failure mechanisms.

Twenty-eight possible collapse mechanisms are established as the most probable according to their statistical occurrence observed in previous earthquake surveys. Seismic vulnerability considerations are therefore linked to a preliminary identification of the active failure mechanism which corresponds to the lowest value of the collapse multiplier.

Whilst the approach proposed by Italian Guidelines is very straightforward, easily applicable by everyone, even not familiar with limit analysis concepts, it has two rather relevant drawbacks. The first is linked to the risk of an overestimation of the horizontal acceleration at failure, because the upper bound theorem of limit analysis is used. The second is related to the utilization of a no-tension material model. As a matter of fact, such assumption is a safe one, but does not take into account some key features playing an important role in the formation of the failure patterns. Among the others, the most important features are the orthotropy at failure and the actual texture, especially along the thickness of the wall. This latter feature considerably influences the monolithic behavior against out-of-plane loads.

In the present paper, with the aim of estimating the ultimate load bearing capacity of the churches, three different approaches are critically compared and systematically applied to the case studies considered.

The first procedure is a global pushover analysis carried out with the commercial code Strand7 [22], where an isotropic elastic-perfectly plastic material model, obeying a Mohr–Coulomb failure criterion, is adopted for masonry.

While the FE pushover model is global, the reproduction of partial failure mechanisms is obviously still possible [7,8], especially when the in-plane stiffness of the floors and the roof is not accounted for.

The second procedure consists of the estimation of the collapse loads by means of pre-assigned failure mechanisms, as per Italian Guidelines on built heritage requirements. A poor interlocking between perpendicular walls is assumed, in agreement with in-situ surveys, with a monolithic behavior along the thickness. This latter hypothesis is justified by the regular texture of the churches, with walls constituted by multi-head clay bricks, with good through-thickness interconnections secured by transversal blocks (diatoni) regularly present.

The major practical drawback of pre-assigned failure mechanisms is the impossibility to automatically interface with previous FE models of the structure, always required when response spectrum analyses are performed.

The third approach supersedes the aforementioned limitations and relies on FE upper bound limit analyses performed on the entire structure. The approach assumes, for the limit analyses, the same FE discretization previously utilized by standard elastic analyses. The code requires a discretization with rigid triangular elements, with possible dissipation for in- and out-of-plane loads on interfaces between adjoining elements. Mechanical properties of the interfaces may be derived either from homogenization procedures, once the actual geometry and the mechanical properties of the constituent materials are known, or using code of practice prescriptions. The proposed approach works easily with relatively refined discretizations and automatically allows the identification of the active failure mechanism. However, still, some drawbacks remain, as for instance the inability to provide clear crack patterns or damage maps (due to the nature of the model utilized, which is rigid-plastic).

All models are tested on seven masonry churches, exhibiting different geometrical features. Detailed comparisons among the active failure mechanisms provided by all models and the corresponding collapse multipliers are discussed.

It is found that, in the majority of the cases, the three approaches provide similar active failure mechanisms and failure accelerations. However, pushover analyses are generally very demanding, requiring much more time to be performed. The procedure based on the assumption of partial failure mechanisms is certainly the most immediate in the processing phase, because it is the trivial application of the principle of virtual works. However, it requires a detailed preparatory work to transfer data between the idealized scheme of the code and the real cases, which have been managed with the help of a 2D CAD software. In addition, it involves some rough assumptions on the acting loads, totally or partially neglecting some effects induced by arches, vaults, roofs, etc. The collapse loads so predicted are always very conservative and much lower when compared with alternative procedures, clearly demonstrating the intrinsic limitations of the approach.

Finally, the third approach (FE limit analysis) always proved robustness, quickly providing active failure mechanisms in acceptable agreement with both alternative procedures and post-earthquake surveys.

2. Modeling strategies and mechanical properties adopted

The group of structures under study is constituted by seven masonry churches, all located near the two epicenters of the major seismic events occurred in May 2012, see Fig. 1.

An indication of the peak ground accelerations (PGA) estimated for the region under consideration is reported in Fig. 2. Data are post-processed from those available from Italian Institute of Geophysics and Volcanology INGV [15,16]. Spectral

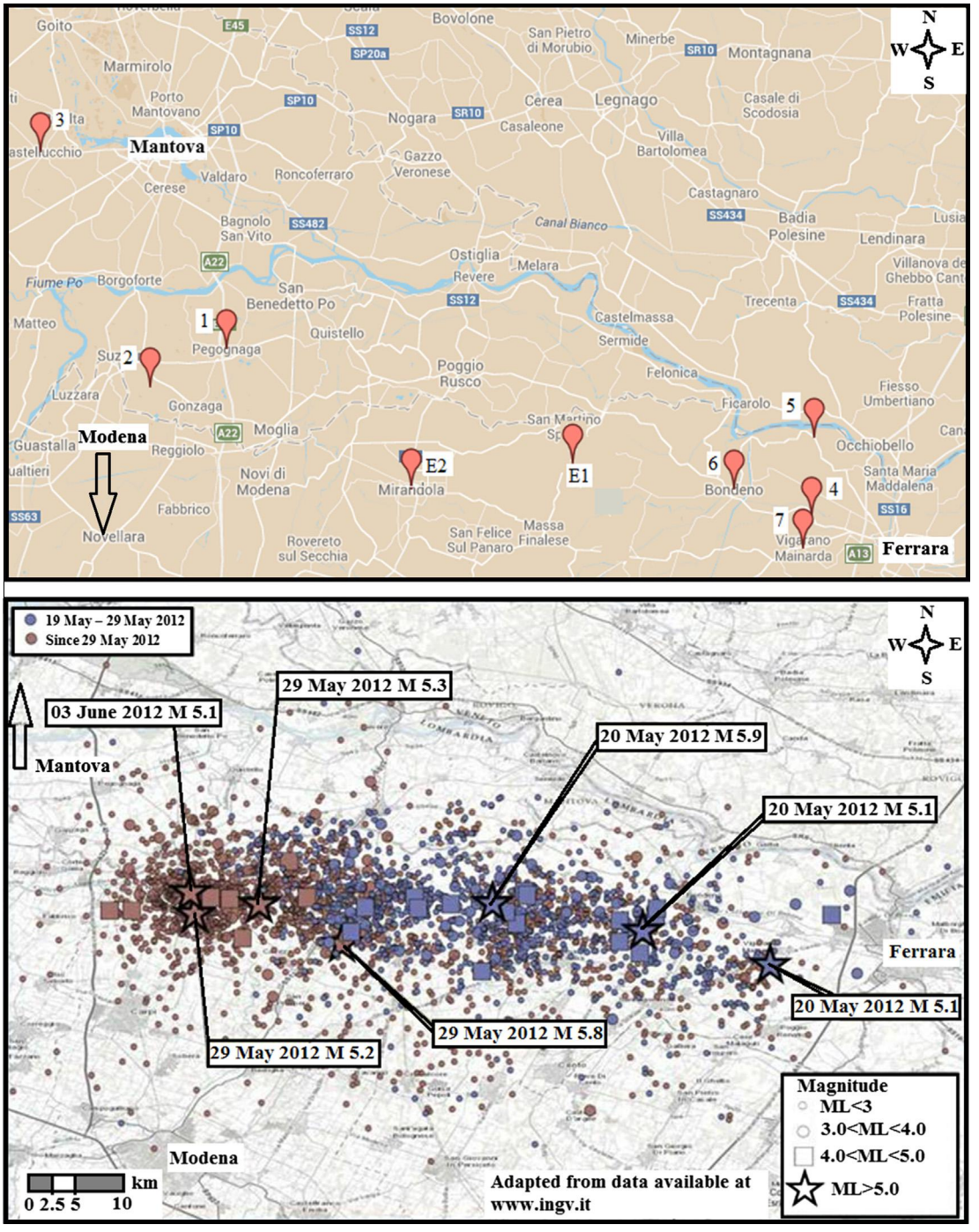

Fig. 1. Location of the churches (E1 and E2 approximately represent the epicenters of M 5.9 and M 5.8 seismic events, respectively) and distribution of the two seismic sequences (blue: 20 May 2012 sequence; red: 29 May 2012 sequence). (For interpretation of the references to color in this figure legend, the reader is referred to the web version of this article.)

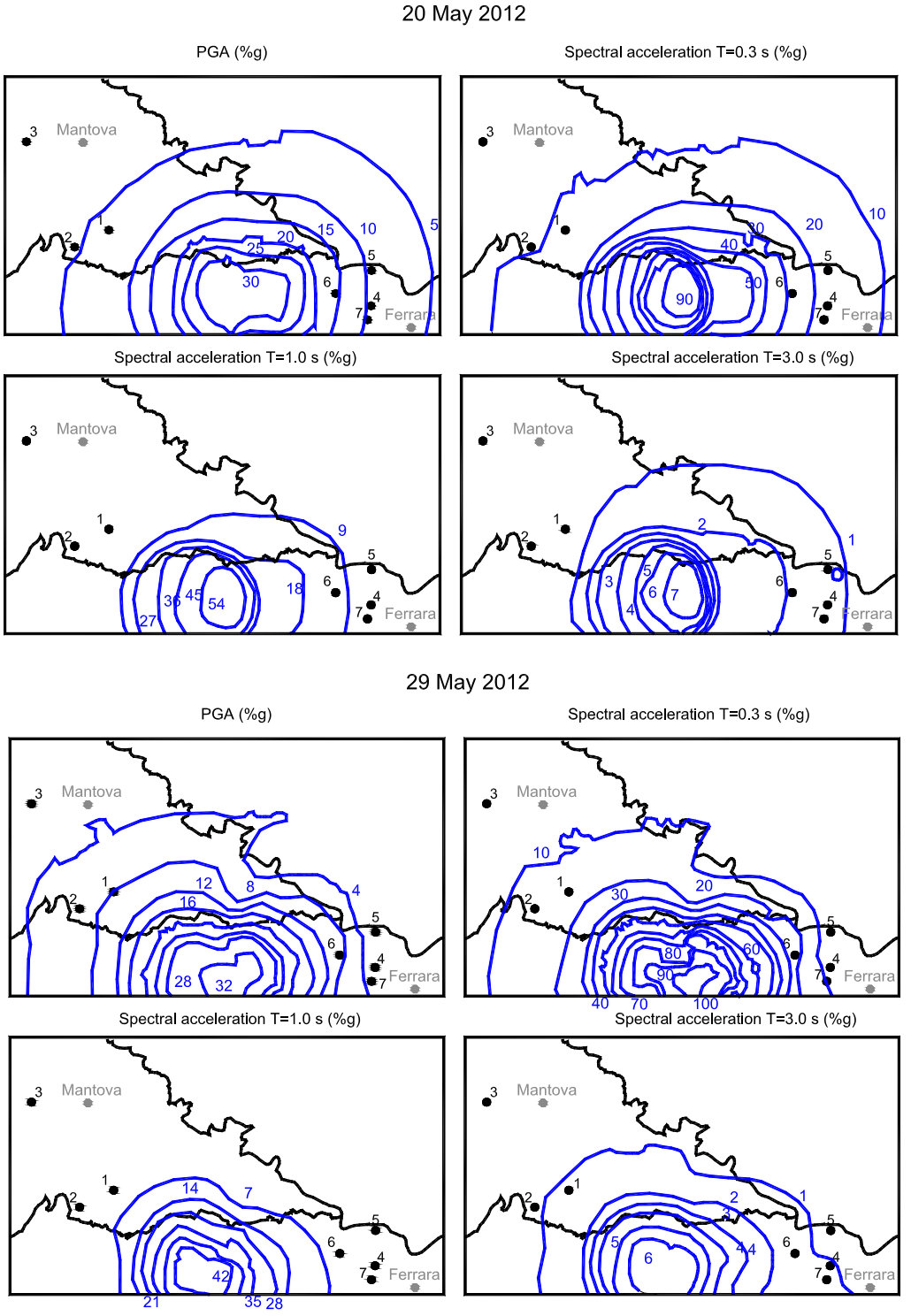

Fig. 2. PGA and spectral accelerations (for three vibration periods of a single-DOF elastic structure), 20th and 29th May 2012 seismic events.

accelerations for main periods of the structure, equal to 0.3, 1.0 and 3.0 s respectively, are also represented. Spectral accelerations are directly collected from INGV post-processed data. INGV obtained such maps from ground acceleration records on a single-DOF elastic system with damping equal to 5%. As can be seen, an amplification of the spectral acceleration (when compared to the PGA) is always experienced for structures with period equal to 0.3 s. Typically, masonry churches under consideration exhibit vibration periods with not negligible participating mass near 0.3 s.

Generally, when dealing with masonry geometry (texture, thickness and along-thickness behavior) and mechanical properties, it is possible to conclude that all the structures exhibit similar features. In particular, the thickness of the load carrying walls ranges between 40 and 100 cm. Masonry is multi-head and is constituted by relatively high resistance clay bricks, texture is regular, with joints thickness approximately equal to 10 mm.

The issue of constituent materials mechanical properties results particularly interesting. It is common opinion, indeed, that the major damages registered by historical buildings, such as towers, castles and churches, are a consequence of the very poor mechanical properties of joints, whereas clay bricks exhibited a quite high strength. Post-collapse surveys and photos taken after the main shocks, where intact stacks of bricks without mortar are visible, fully support this conclusion.

In absence of ad-hoc experimental campaigns performed on the case studies at hand, it is necessary to refer to what stated by Italian Code for existing masonry buildings.

As a matter of fact, masonry is a material which exhibits distinct directional properties due to the mortar joints, acting as planes of weakness. Depending on the level of accuracy and the simplicity desired, it is possible to use the following modeling strategies:

- *Micro-modeling*. Units and mortar in the joints are represented by continuum elements, whereas the unit mortar interface is represented by discontinuous elements. To limit the computational effort in simplified micro-modeling, units are expanded and modeled by continuum elements, whereas the behavior of the mortar joints and unit-mortar interface is lumped in discontinuous elements. For the problem at hand, micro-modeling is inapplicable, due to the need of limiting the degrees of freedom in the non-linear analyses.
- *Homogenization*. It replaces the complex geometry of the basic cell using, at a structural level, a fictitious homogeneous orthotropic material, with mechanical properties deduced from a suitable boundary value problem solved on a suitable unit cell, which generates the entire structure by repetition. For the problem at hand, where multi-head walls are present, the identification of a unit cell is however questionable and the utilization of orthotropic models would complicate the structural analysis without a hypothesis sufficiently based on the actual texture present.
- *Macro-modeling*. Units, mortar and unit-mortar interface are directly smeared into a continuum (either isotropic or orthotropic), with mechanical properties deduced at the micro-scale by means of available experimental data. This latter approach is probably the most suitable for reliable large scale computations. However, it would require a preliminary geometrical and mechanical characterization which, in this specific case, would entail costly and time consuming experimental campaigns to fit the several material coefficients needed to perform realistic analyses.

All these features considered, in what follows, isotropic macro-models are used for masonry. The reason for adopting an isotropic material stands in the impossibility to evaluate many parameters necessary for anisotropic materials in the inelastic range, in absence of ad-hoc experimental characterizations. Finally, it is worth noting that commercial codes rarely put at disposal to users anisotropic mechanical models suitable to describe masonry with regular texture in the non-linear range.

According to Italian Code NTC 2008 [23], Chapter 8, and subsequent Explicative Notes [24], the mechanical properties assumed for masonry material depend on the so-called knowledge level LC, which is related to the so-called Confidence Factor FC. There are three LCs, labeled from 1 to 3, related to the knowledge level about the mechanical and geometrical properties of the structure. The knowledge level LC3 is the maximum, whereas LC1 is the minimum. For the case at hand, a LC1 level is assumed in absence of specific in-situ test results.

Confidence Factor FC summarizes the knowledge level regarding the structure and the foundation system, from a geometric and mechanical point of view. It can be determined defining different partial confidence factors FCk (k = 1,4), on the basis of some numerical coefficients present in Italian Code (Table 4.1 Italian Guidelines). Due to the limited knowledge level achieved in this case, the highest confidence factor (FC = 1.35) was used.

After visual inspections, the values adopted for cohesion and masonry elastic moduli are taken in agreement with Table C8A.2.1 of the Explicative Notes [24], assuming a masonry typology constituted by clay bricks (a so-called Ferraresi bricks typology is present in all cases, with approximate dimensions equal to $300 \times 60 \times 100$ mm^3) with very poor mechanical properties of the joint and quite regular courses.

With the lowest knowledge level LC (confidence factor FC = 1.35), Italian Code requires to select, in Table C8A.2.1, the lower bound values for strength and the average values between lower and upper bound for elastic moduli.

Pushover analyses are conducted using Strand7 [22] with an elastic perfectly plastic material obeying a Mohr–Coulomb failure criterion. A friction angle equal to 30° is assumed, again in agreement with some considerations deduced from the Italian Code. The utilization of perfectly plastic materials is allowed by Italian Guidelines when masonry is modeled with 2D and 3D finite elements, i.e. where the drop of the pushover curve for the reduction to a single-DOF system with the area equivalence is hardly reproducible. In this case, Italian Guidelines recommend carrying out analyses up to "meaningful displacements", which may be reasonably associated with an activation of the failure mechanism.

Mechanical properties assumed in all cases for the pushover simulations are summarized in Table 1. When dealing with limit analysis, a tension cut-off equal to $0.25c$, where c is the cohesion, is also hypothesized, with the aim of simulating a "quasi" no-tension material within a linear programming approach. Finally, limit analysis with pre-assigned failure mechanisms works within the no-tension material hypothesis.

It is interesting to notice that, according to Table 1, mechanical properties assumed for masonry in the pushover analysis exhibit a quite high cohesion, apparently not in agreement with Table C8A.2.1 indications. However, with the aim of

Table 1
Mechanical properties assumed for masonry in all the cases analyzed.

Material	Cohesion c (MPa)	Internal friction angle (°)
Masonry bricks with lime mortar joint	0.15	30

analyzing the structure in the most favorable case, all the possible improving hypotheses are adopted, as for instance thin mortar joints, mortar with good mechanical properties and presence of good interconnections. When each one of the previous properties holds, an increasing parameter that multiplies the table value can be introduced, allowing for the utilization of the high cohesion reported in Table 1. The final aim is to demonstrate that, albeit mechanical properties are the highest that can be adopted in practice, the churches still remain particularly vulnerable to horizontal actions.

Finally, it is worth emphasizing that for all the analyzed churches, light wooden roofs are present, in agreement with the building traditional technology of such typology of structures in the region considered. Their membranal stiffness is safely assumed negligible for horizontal loads, as well as the box behavior induced by their presence in the FE models. For this reason, only vertical loads transferred by the roof to the head of perimeter walls are introduced in the models.

3. Brief description of the churches under study

Some rough sketches of the structures under consideration are reported from Figs. 3–9, with an approximate indication of the dimensions of the churches and their FE discretizations. The reader interested in a detailed description of the geometry and a survey of the damages observed after the seismic events is referred to [25].

Hereafter, only a concise description of the churches is provided case by case.

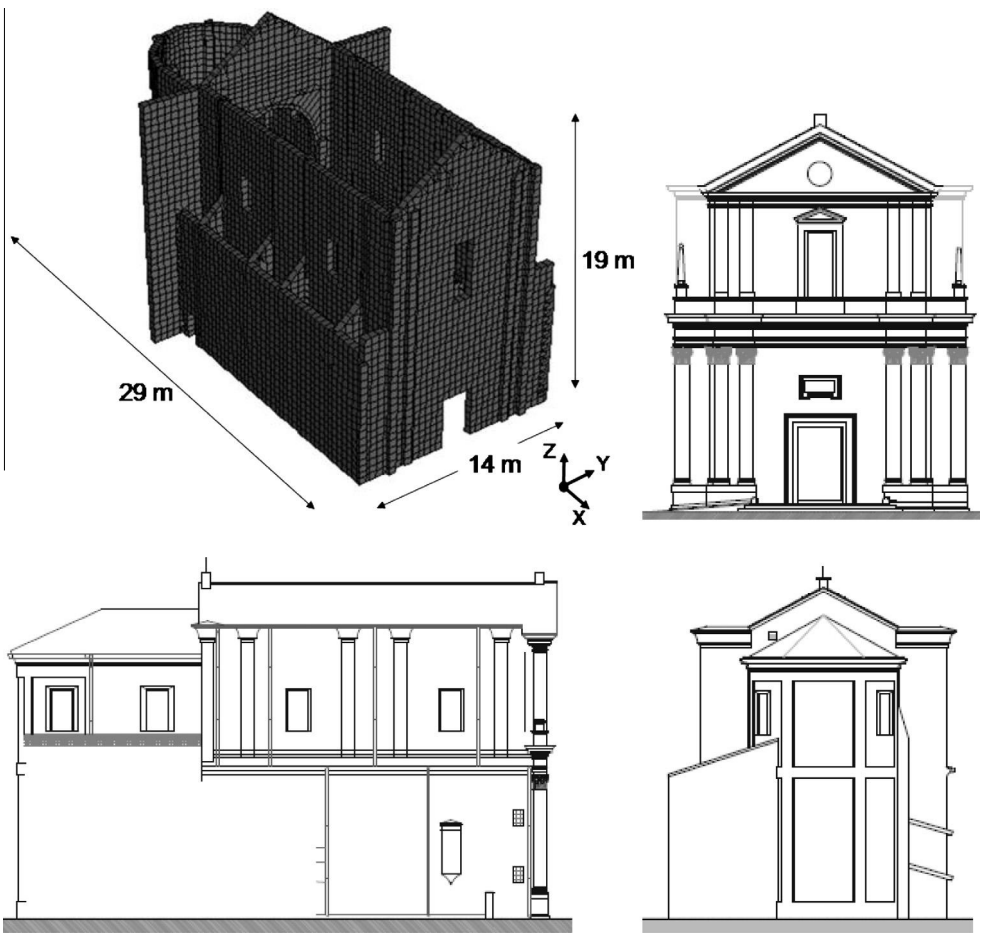

Fig. 3. Church 1, San Giacomo Maggiore Apostolo in Pegognaga.

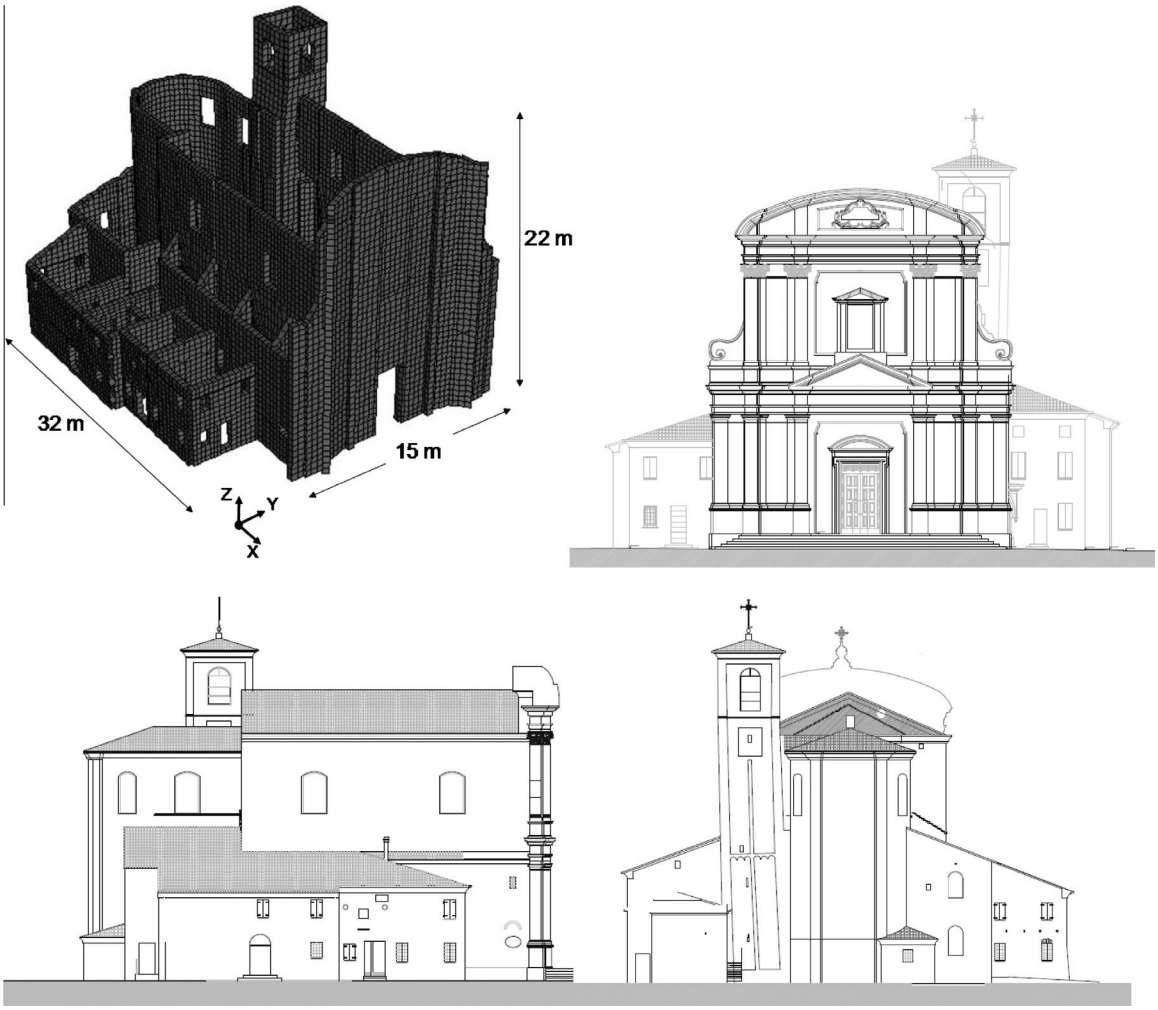

Fig. 4. Church 2, San Sisto II in Palidano di Gonzaga.

- Church 1, San Giacomo Maggiore Apostolo in Pegognaga, Fig. 3. This church is a structure with single nave and small lateral chapels, approximately 29 m long. The central nave has a width equal to 9.30 m and a length of 18 m. The presbytery has rectangular shape, is 5.80 m long and ends with a circular apse. On both sides along the central nave, symmetrically placed, there are four chapels, 1.80 m large and 4.75 m long. A timber roof is present and is carried by a wooden truss-like structure.
- Church 2, San Sisto II in Palidano di Gonzaga, Fig. 4. This church is a single nave structure, with a wide presbytery and a façade exhibiting an unusual concave shape. The nave has a length equal to approximately 22 m. The maximum height of the façade is equal to 22 m. Four chapels subdivide the internal space and globally make larger the overall width of the structure. The apse is circular, with height equal to 13.50 m, and is structurally linked to the presbytery, that is 6 m long. The bell tower, survived the demolition of an old church, and results incorporated into the new building. It exhibits a quite marked inclination that increased in the last few years, as a consequence of some foundation settlements, typical for soils of this region under tall structures with relatively small foundations. The global plant of the aggregates results rather complex, as a consequence of the presence of different buildings (as for instance the old rectory, the sacristy, a small theater with the oratory, etc.) incorporated into the church. The wooden roof is carried by a classic wood truss-like structure. Some masonry stiffening columns, with a rectangular section equal to 80×60 cm, are placed inside the church, in adhesion to perimeter walls. Such columns traditionally have the main function to better diffuse vertical loads transferred by the roof, because churches are not conceived to withstand horizontal loads. They contribute in a negligible manner to the increase of the overall load bearing capacity under seismic actions. This notwithstanding, they have been modelled by means of 2D FEs with equivalent thickness, in order to obtain a FE discretization much closer to the reality.

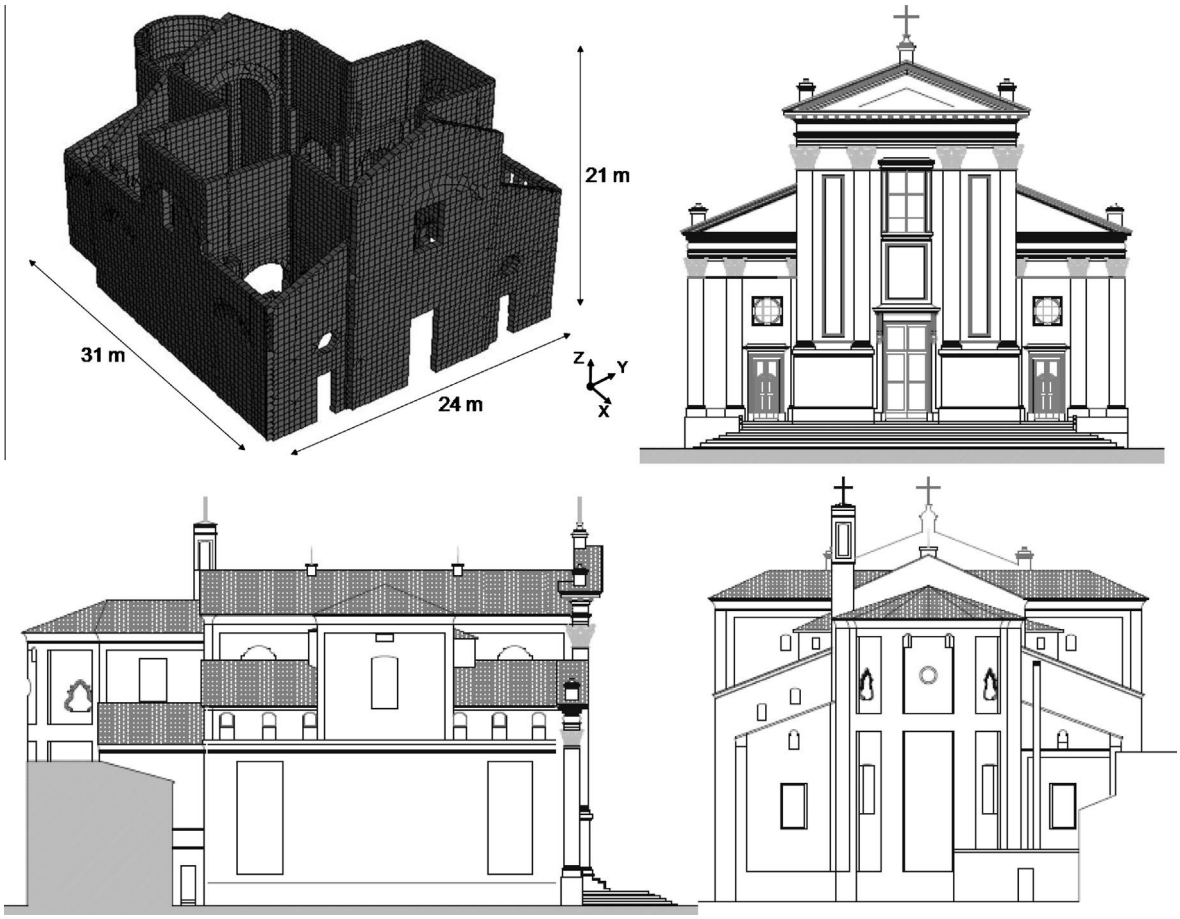

Fig. 5. Church 3, San Giorgio Martire in Castellucchio.

- Church 3, San Giorgio Martire in Castellucchio, Fig. 5. The structure exhibits a Greek cross plan, degenerating into a rectangle with a length equal to 31.5 m and with a 23.7 m wide transept. The internal space is characterized by the presence of four large columns carrying a central vault. The intersection of the naves with the transept architecturally defines four distinct zones, apart the center surmounted by the vault, with attached much smaller volumes containing a corresponding number of minor altars. The church presents different heights; the central vault reaches a height equal to 15.7 m, while the four lateral zones are 8 m high. The thickness of the external walls is 60 cm. The façade is a typical Romanesque one and has a thickness equal to 70 cm.
- Church 4, Santi Pietro e Paolo in Vigarano Pieve, Fig. 6. This church consists of different units independently built in different times and then put together. The dimensions in plan are 29.87 m $\times$ 17.1 m. A single nave is present, with smaller chapels attached laterally. The presbytery, ending with a circular apse, has a length equal to 9.64 m and a width equal to 4.69 m near the triumphal arch, which enlarges to 6.57 m in correspondence of the apse. The thickness of the church walls is obviously larger than that of the annex buildings. The perimeter walls present only a few windows. A wooden beam structure carries the timber roof. The height of the lateral walls of the single nave is equal to 11.20 m and decreases up to 8.10 m in correspondence of the presbytery. The façade is 17.1 m wide and it reaches a height equal to 18.30 m. The bell tower, with a square shape in plan, presents a height equal to 24.47 m and is incorporated into the church.
- Church 5, Santi Filippo e Giacomo in Ravalle, Fig. 7. This church has an unusual shape when compared to other similar structures located in the same region (Pianura Padana). There is a very long presbytery (about 12 m long), not particularly large (6 m). The architectural system is constituted by a single quite wide central nave, where no change of the roof shape at the interconnection with presbytery and lateral chapels is observed. The apse is circular and naturally closes the long presbytery. There are three quite large windows, which internally allow a good lighting of the church, on each lateral wall of the nave and other two openings on the apse. The maximum height of the church is rather constant (13.76 m). The façade is 19.41 m high and 15.11 m wide, and exhibits a typical XVII century architectural style, quite common for churches built in the same period in the area.

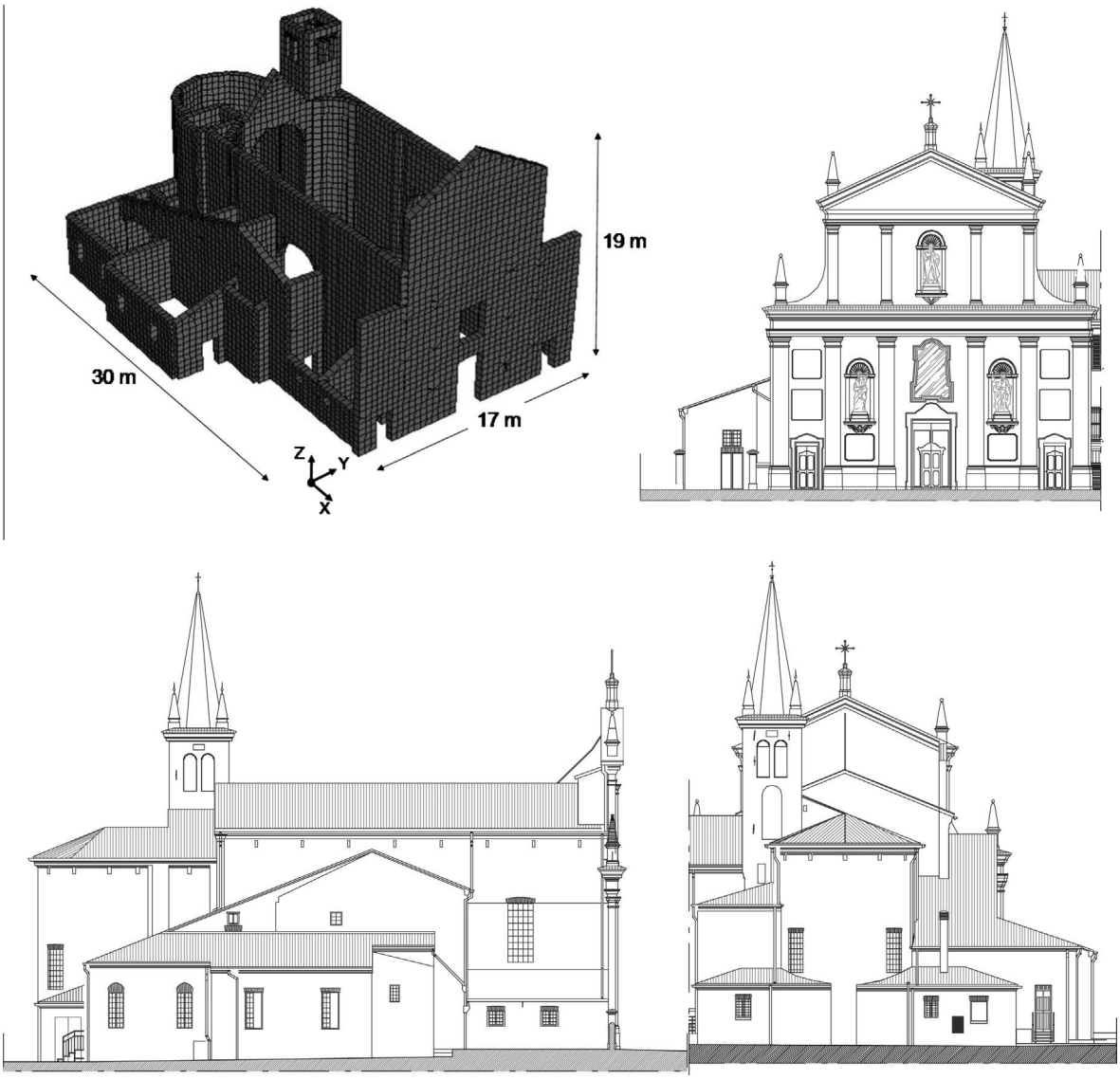

Fig. 6. Church 4, Santi Pietro e Paolo in Vigarano Pieve.

- Church 6, Natività di Maria Vergine in Bondeno, Fig. 8. This church is a single nave structure with continuous lateral chapels, approximately 36 m long and 22 m wide. The façade, 19 m high, is built with a typical Romanesque style; however, almost the whole of the structure, except the apse, which dates back to the Middle Age (1200), was built within the two decades 1870–1890. The bell tower, almost totally isolated from the church (except a very small corridor of interconnection at the ground floor level) was readapted in XIII century on an earlier military tower belonging to the ancient external walls of the town, then demolished. A light wooden roof carried by a steel truss structure (installed at the beginning of the 20th century) covers the central nave and the chapels, whereas the ancient apse is surmounted by peculiar irregular gothic cross vaults.
- Church 7, Natività della Beata Maria Vergine in Vigarano Mainarda, Fig. 9. This church is a structure constituted by three naves, with approximate dimensions equal to 31 m $\times$ 20 m $\times$ 13 m (length $\times$ width $\times$ maximum height). A simple system of five transversal arches, similar to triumphal arch systems and equally spaced each 5 m, transversally interconnects the lateral walls to the central nave, thus making the behavior of the church more global when compared with other typical structures of this region. The façade, however, results poorly interconnected with perpendicular walls, thus making the hypothesis usually done in global finite element analyses (perfect interconnection among transversal walls) rather questionable. The lateral walls of the central nave result highly perforated, both for the presence of large openings surmounted by arches interconnecting central and lateral naves and for the presence

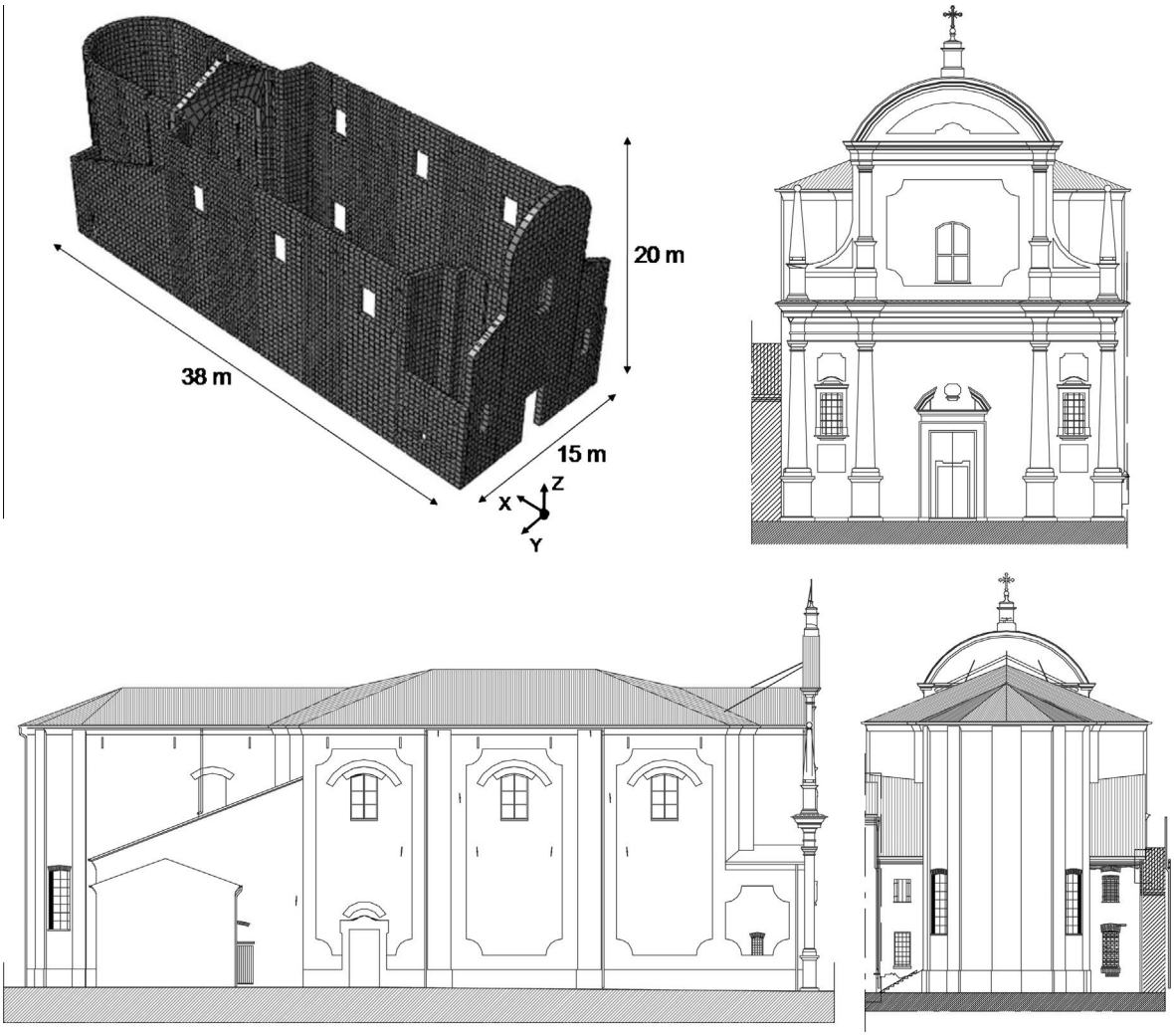

Fig. 7. Church 5, Santi Filippo e Giacomo in Ravalle.

of relatively large windows in the upper part. The church is connected in the rear to a secondary sacristy on the left and to a large oratory on the right; only a part of this latter structure is considered in the FE model, since the focus remains the analysis of the church.

4. Observed damages

A concise overview of the damages suffered by the different churches during the 2012 Emilia-Romagna seismic sequence is provided.

- Church 1: Damage suffered by the Church 1 is a visible detachment of the façade from the perpendicular walls, which suggesting a partial activation of a first mode of collapse. On the other hand, a deep vertical crack is present in the middle of the façade, linked to the formation of a vertical yield line. A visible nearly vertical crack pattern is present in the bell tower. Lateral walls of the single nave were severely cracked in the upper part, with visible residual out-of-plane displacements, probably related to the activation of an out-of-plane mechanism of the lateral walls, see Fig. 10a.
- Church 2 was severely damaged, with visible and diffused crack patterns on the façade and the apse. In particular, the façade exhibits the activation of a vertical yield line, symmetrically placed and developing from the main entrance to the tympanum. Moreover, deep cracks are present on lateral walls, at the interconnection with the façade, again showing the partial activation of an out-of-plane mechanism for the façade, see Fig. 10b. Lateral walls present cross

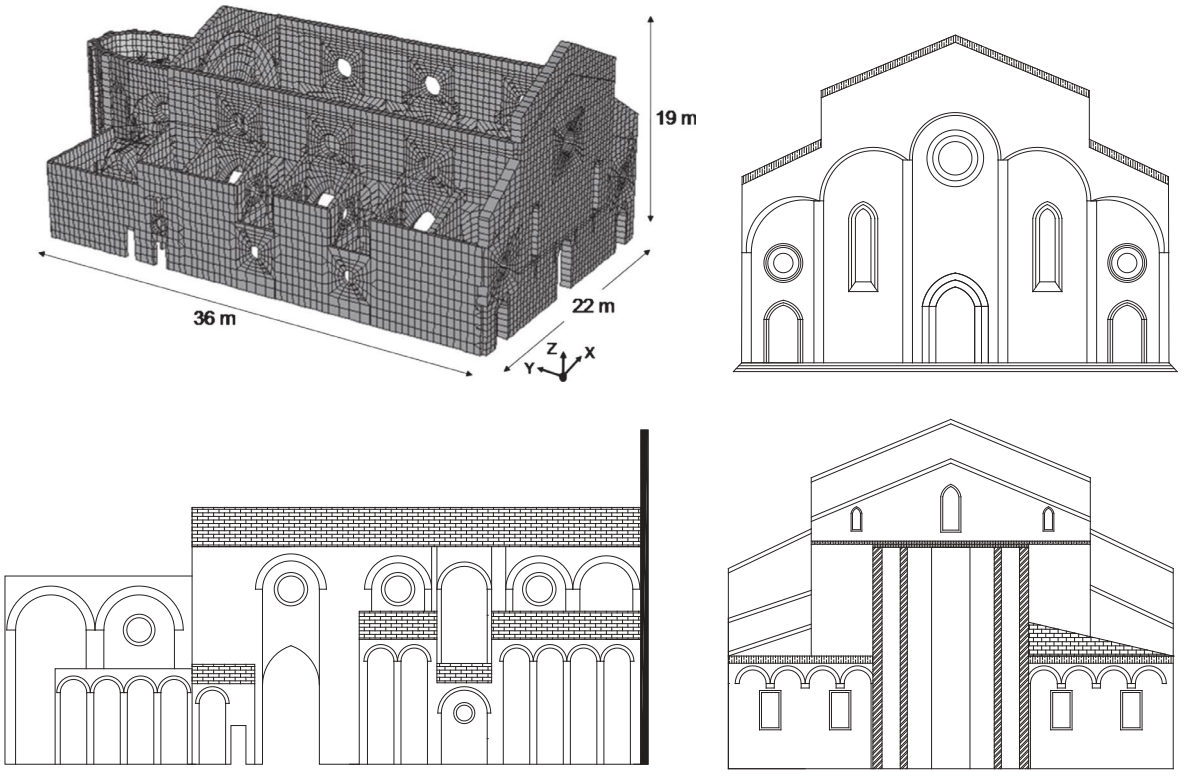

Fig. 8. Church 6, Natività di Maria Vergine (Duomo) in Bondeno.

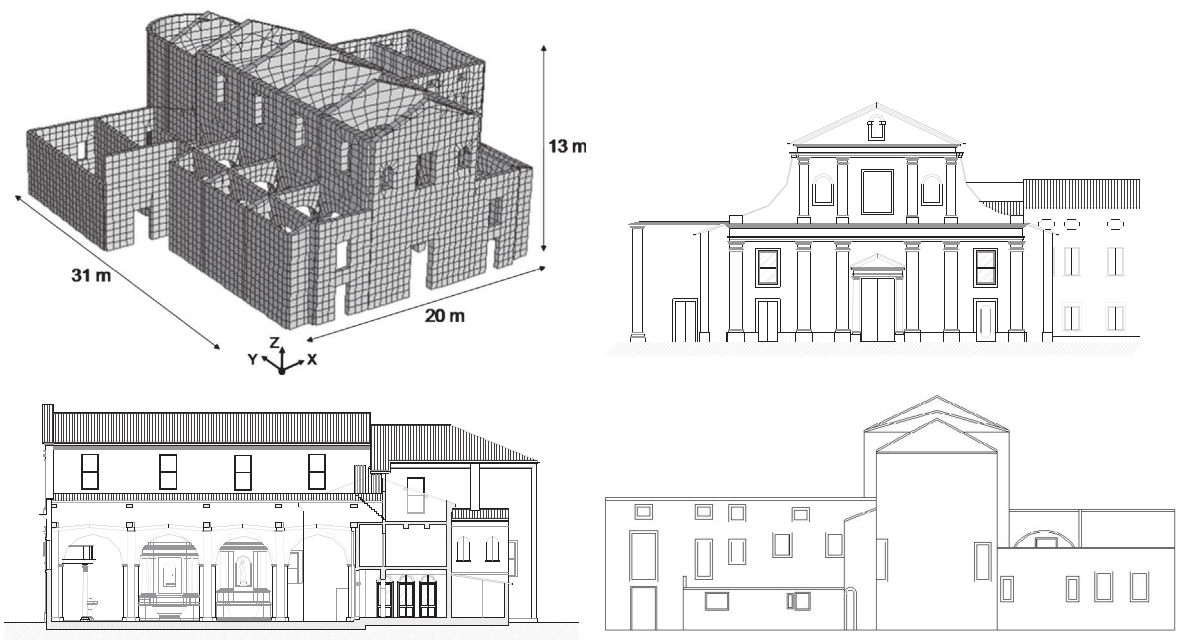

Fig. 9. Church 7, Natività della Beata Maria Vergine in Vigarano Mainarda.

cracks on spandrels, visible on both sides, which are typical of an in-plane shear failure of the structural element. The apse clearly exhibits the partial activation of an overturning mechanism with cylindrical hinge forming near the base, which is typical for such kind of structures.

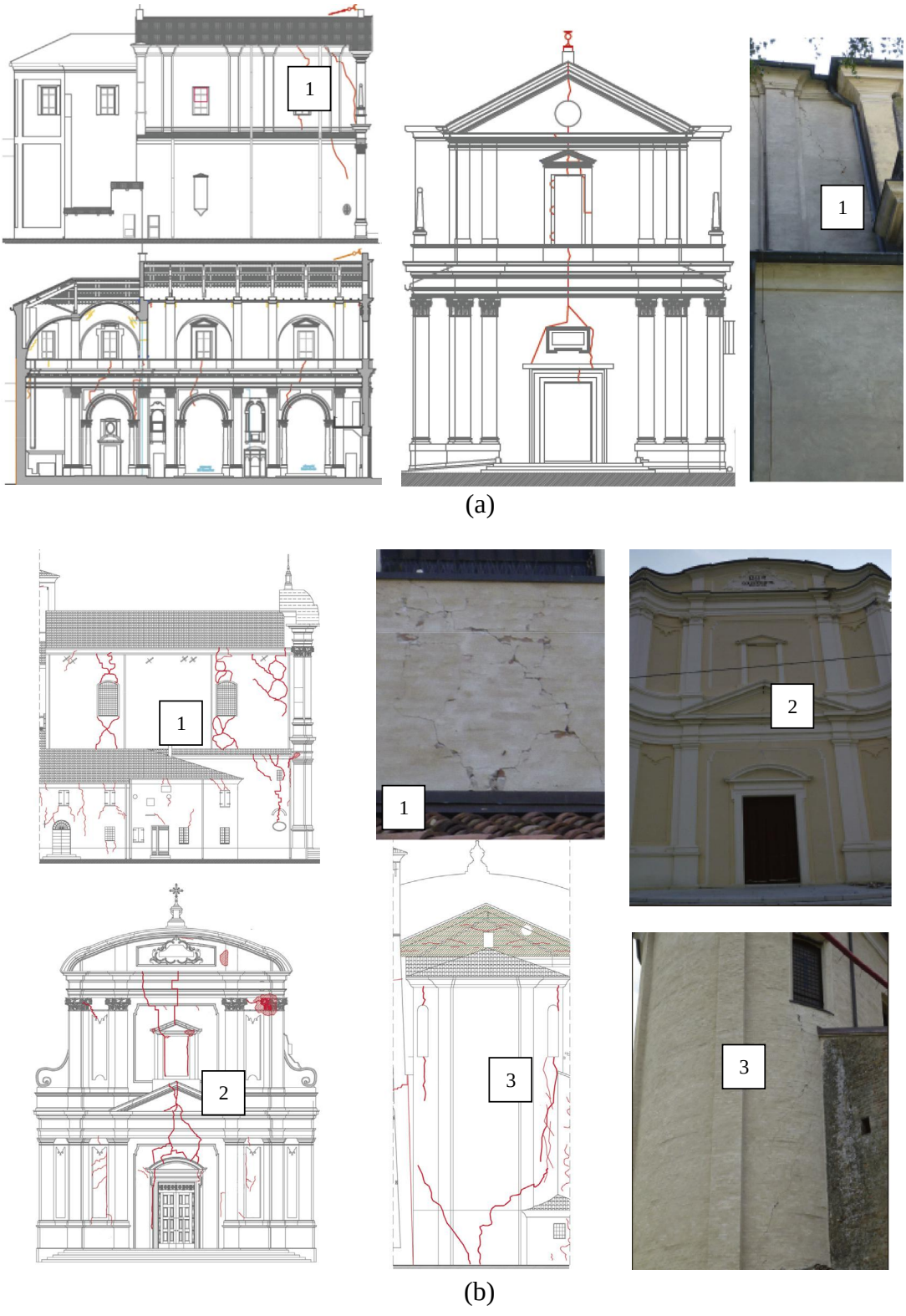

Fig. 10. Crack patterns induced by the seismic sequence. (a) Church 1. (b) Church 2.

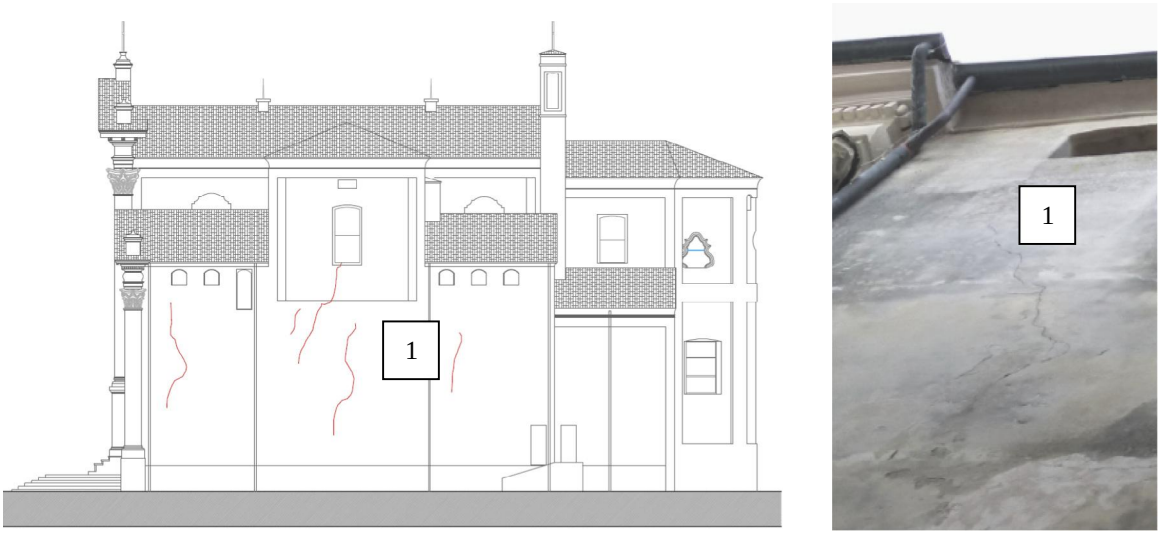

(a)

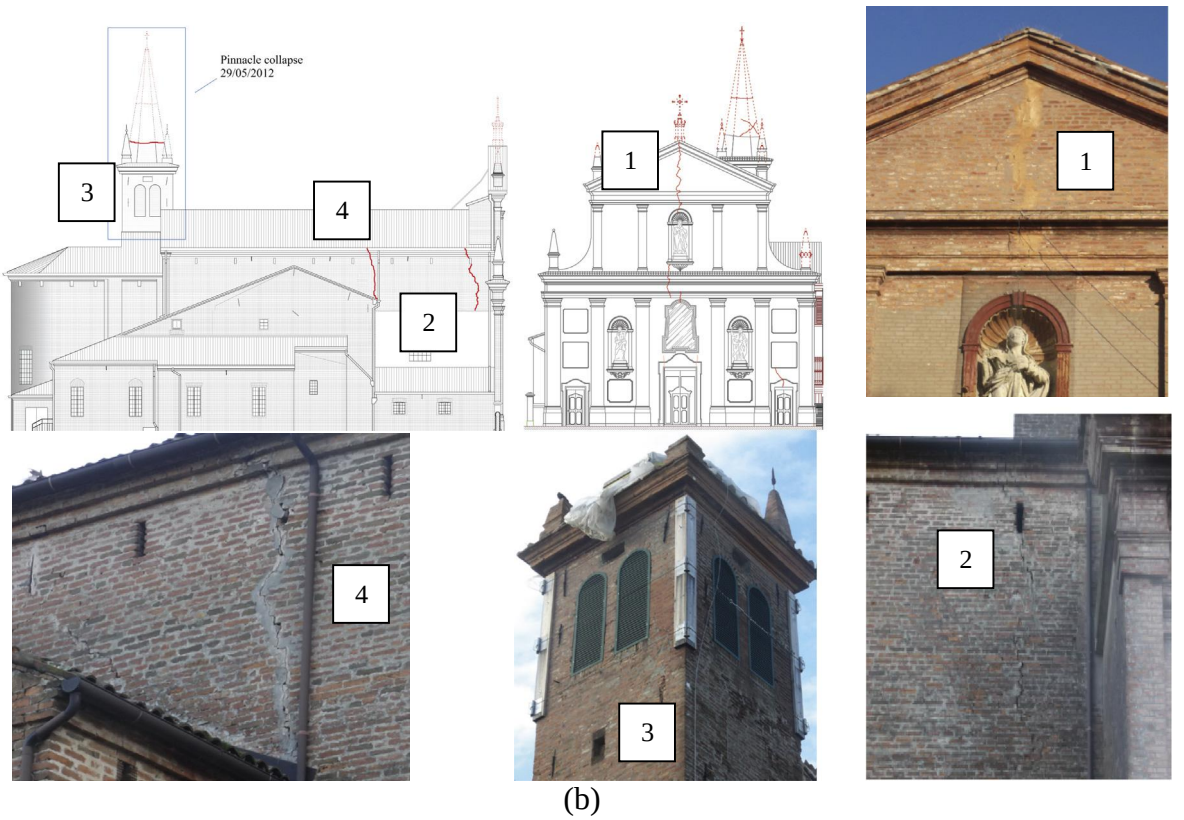

(b)

Fig. 11. Crack patterns induced by the seismic sequence. (a) Church 3. (b) Church 4.

- Church 3 presents less marked damages, because of its geographical position, sufficiently far from the epicenters of the seismic events. However, the lateral walls exhibit, on the external surface, quite visible almost vertical cracks at the mid span and near the vertical supports, represented by the façade and the triumphal arch, suggesting the partial activation of an out-of-plane mechanism, see Fig. 11a.

- Church 4, see Fig. 11b, suffered severe damages on the façade, with the formation of a continuous, vertical and deep crack running on the overall façade length and again suggesting the activation of the overturning of the façade into two macro-blocks. The pyramidal pinnacle of the bell tower collapsed during the second seismic event, a consequence typically linked to its unusual shape and the almost absence of vertical pre-compression. Two deep almost vertical cracks are also present on the lateral walls, one in correspondence of the intersection with the façade, the other at the middle span. While the first crack suggests a partial detachment of the façade from the lateral walls, indicating that, despite the good interconnection, the tympanum tends to overturn out-of-plane with the formation of a cylindrical hinge forming at an intermediate height, the second crack is more related to the out-of-plane behavior of the lateral walls. The sacristy, forming a complex annex of smaller buildings, was severely damaged and exhibits a complex pattern of cracks clearly ascribed to the limited shear strength of the walls. Some minor cracks are present in the apse too.
- Church 5, see Fig. 12a, suffered major damages located on lateral walls, near the façade, indicating an overturning of the upper part (the heavy 3 m high tympanum may be structurally regarded as a cantilever beam) of the façade and shear diagonal cracks, especially in correspondence of the windows.
- Church 6, see Fig. 12b, shows a partial detachment of the façade from lateral walls, again suggesting the overturning of the structural element, as well as shear cracks on the apse and the vaulted system covering the apse. A clear detachment of some lateral chapels is observed, evidently due to the insufficient interconnection between nave walls and chapels.
- Church 7, see Fig. 12c, presents a fully active first mode failure mechanism on the façade, with visible overturning along a straight horizontal yield line. In correspondence of the upper part, the façade shows a large detachment from lateral walls, with displacements exceeding 30 cm, also demonstrating the rather poor interconnection between perpendicular walls. The apse exhibits an almost active failure mechanism, with the formation of a 45° inclined crack departing from the upper part and developing for a couple of meters. The failure mechanism, albeit not fully active, suggests the out-of-plane rotation of a portion of the apse around a horizontal hinge placed in correspondence of the middle height.

5. FE upper bound limit analysis code: a brief overview

The FE code utilized in this study is explicitly devoted to the analysis of large-scale monuments and it is a simplified version of the model proposed by Milani and co-workers, see [7–9,26–31]. The structure is discretized by means of rigid-infinitely resistant triangles. For each element, only six optimization variables (centroid velocities $\mathbf{u}^E = [\,u_x \quad u_y \quad u_z\,]^T$ and rotation rates around centroid $\mathbf{\Phi}^E = [\,\Phi_x \quad \Phi_y \quad \Phi_z\,]^T$) are needed (Fig. 13). Hence, plastic dissipation is allowed only at the interface between adjoining elements. Element variables are collected in the 6×1 vector $\mathbf{w}^E = [\,\mathbf{u}^{E^T} \quad \mathbf{\Phi}^{E^T}\,]^T$. Considering an interface I between elements N and M, with connecting nodes A and B, the local frame of reference **s–t–n** is found as follows (Fig. 13):

$$\mathbf{s} = \frac{A-B}{\|A-B\|} \quad \mathbf{n}_1 = \frac{D_1 - D_2}{\|D_1 - D_2\|} \quad \mathbf{t}_1 = \mathbf{n}_1 \times \mathbf{s} \quad \mathbf{t} = \frac{\mathbf{t}_1}{\|\mathbf{t}_1\|} \quad \mathbf{n} = \mathbf{s} \times \mathbf{t} \tag{1}$$

where **s** coincides with the interface direction, **n** is perpendicular to the interface and lies in the middle plane between elements N and M planes and **t** is perpendicular to both **s** and **n**. Plastic admissibility is allowed at each internal interface between contiguous elements only in the centroid C of the interfaces, Fig. 13. We denote with $[\mathbf{w}_I] = [\,\Delta w_s \quad \Delta w_t \quad \Delta w_n \quad \Delta\Phi_s \quad \Delta\Phi_t \quad \Delta\Phi_n\,]^T$ the generalized velocity jump vector of the interface I centroid. With reference to Fig. 13c, $[\mathbf{w}_I]$ collects three jumps of velocities of point C along the local frame of reference **s–t–n** (Δw_s, Δw_t, Δw_n) and three rotation rates along axes **s–t–n** ($\Delta\Phi_s$, $\Delta\Phi_t$, $\Delta\Phi_n$). Internal actions associated with the generalized jump of velocities may be collected in the vector $\mathbf{N}_I = [\,V_s \quad V_t \quad N \quad M_s \quad M_t \quad M_n\,]^T$ where V_s, V_t and N are in-plane shear, out-of-plane shear and membrane normal action, respectively, and M_s, M_n and M_t are the out-of-plane bending moment, torsion and in-plane bending moment, respectively. Strength values associated with each internal action are collected in the 12×1 vector $\mathbf{N}_I^0 = [\,V_s^{0+} \quad V_t^{0+} \quad N^{0+} \quad M_s^{0+} \quad M_t^{0+} \quad M_n^{0+} \quad V_s^{0-} \quad V_t^{0-} \quad N^{0-} \quad M_s^{0-} \quad M_t^{0-} \quad M_n^{0-}\,]^T$ representing shear, membrane action, bending moment and torsion resistances, where the superscripts + and − indicate positive and negative (with respect to the local frame of reference) resistance values. Ultimate masonry strengths V_s^0, V_t^0, N^0, M_s^0 and M_t^0 are evaluated through homogenization. In general, they depend on the orientation of the interface and, for V_s^0, V_t^0, M_s^0 and M_t^0, on the vertical pre-compression. In the deformation process, it is assumed that pre-compression remains constantly equal to that evaluated through an elastic analysis under vertical loads only. While this hypothesis is theoretically debatable, it is usually adopted by many authors (e.g. [31]). Finally, components of the vector $\mathbf{N}_I^0$ are evaluated, interface by interface, by a procedure similar to that utilized in [30].

In order to check plastic admissibility on interface centroid, only 12 plastic multipliers per interfaces are required. In detail, six equality constraints in the following form are written:

$$\mathbf{A}_{11}^{eq}\mathbf{w}^M + \mathbf{A}_{12}^{eq}\mathbf{w}^N + \mathbf{I}(\dot{\lambda}_I^+ - \dot{\lambda}_I^-) = \mathbf{0} \tag{2}$$

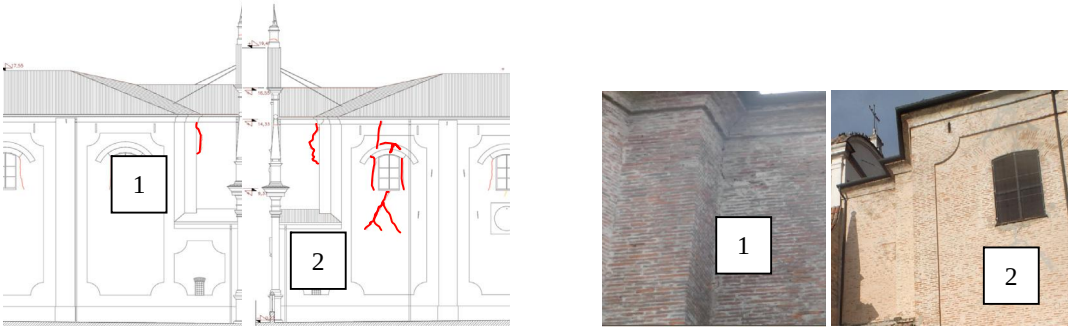

(a)

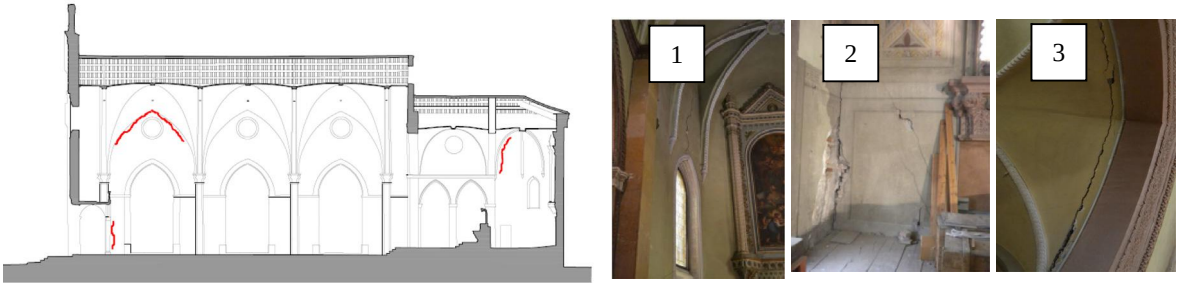

(b)

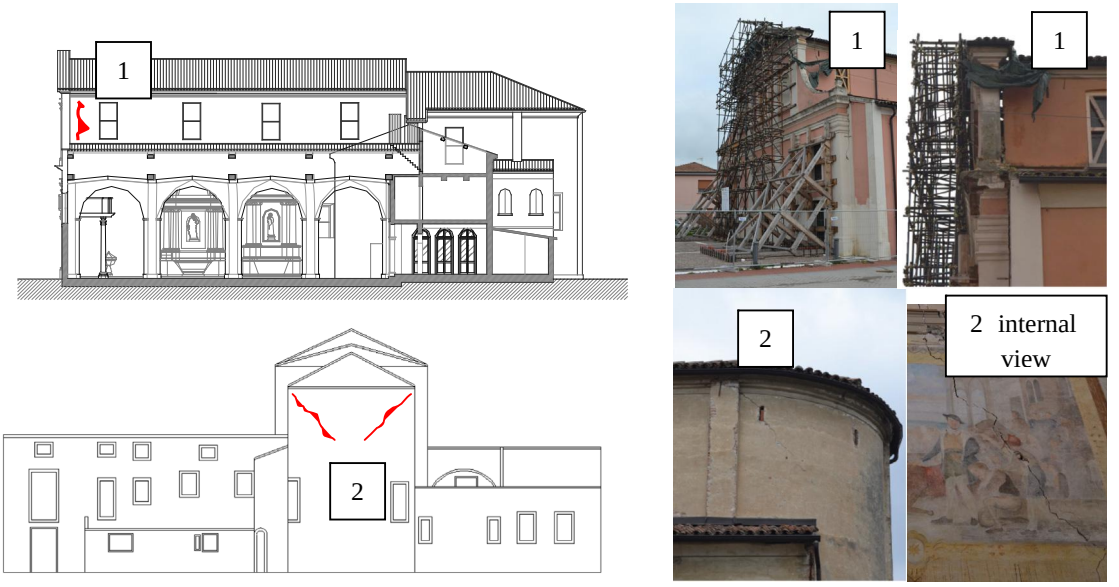

(c)

Fig. 12. Crack patterns induced by the seismic sequence. (a) Church 5. (b) Church 6. (c) Church 7.

In Eq. (2) $\mathbf{w}^M$ and $\mathbf{w}^N$ are the 6×1 vectors that collect velocities and rotation rates of elements M and N, respectively, $\mathbf{A}_{1j}^{eq} \quad j = 1,2$ are 6×6 matrices which depend only on the interface orientation Ω^I and on elements M and N geometry, $\mathbf{I}$ is the 6×6 identity matrix, $\dot{\lambda}_I^+$ and $\dot{\lambda}_I^-$ are 6×1 vectors of the positive and negative plastic multipliers (one positive and one negative multiplier for each internal action). The total internal power dissipated P^{in} is constituted only by the sum of the power dissipated on each interface P_I^{in}. This P_I^{in} can be estimated as $P_I^{in} = \Gamma_I \mathbf{N}_I^0 [\dot{\lambda}_I^+ \quad -\dot{\lambda}_I^-]^T$, with Γ_I = interface length. Boundary conditions are similarly applied to standard elastic FEs and lead to further equality constraints on the structure.

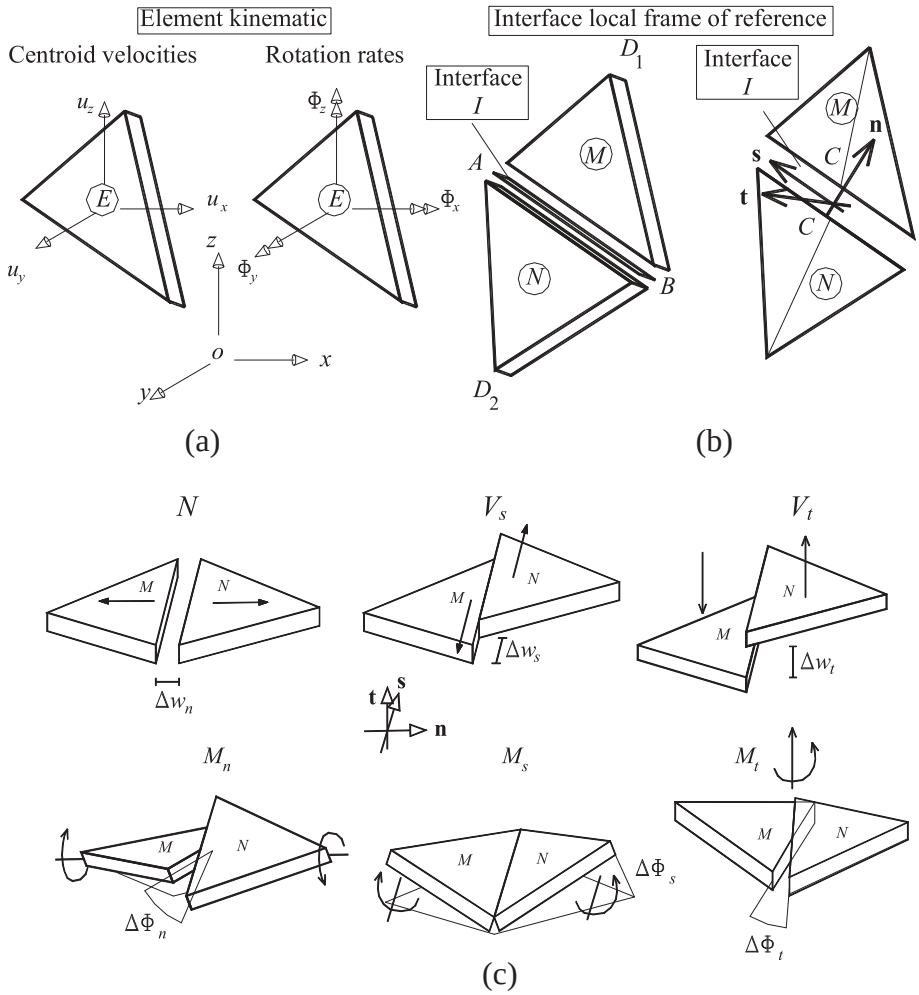

Fig. 13. (a) Triangular plate and shell element used for the upper bound FE limit analysis, element kinematics. (b) Interface *I* local frame of reference. (c) Possible elementary deformation modes (jump of velocities) occurring on an interface *I* between two adjacent elements *M* and *N*.

After the imposition of the well-known "normalization condition" on the external power depending on collapse multiplier, a linear programming problem is obtained, see e.g. [31], where the objective function is represented by the difference between the total internal power dissipated and the external power expended by loads independent of the limit multiplier:

$$\min\left\{\sum_{I=1}^{n^I} P_I^{in} - \mathbf{P}_0^T\mathbf{w}\right\} \quad \text{such that} \quad \begin{cases} \mathbf{A}^{eq}\mathbf{U} = \mathbf{b}^{eq} \\ \dot{\boldsymbol{\lambda}}^{+,ass} \geqslant \mathbf{0} \quad \dot{\boldsymbol{\lambda}}^{-,ass} \geqslant \mathbf{0} \end{cases} \tag{3}$$

In Eq. (3) **U** is the vector of global unknowns, summing the vector of assembled elements velocities and rotation rates (**w**) and the vector of assembled interfaces plastic multiplier rates ($\dot{\boldsymbol{\lambda}}^{+,ass}$ and $\dot{\boldsymbol{\lambda}}^{-,ass}$). $\mathbf{A}^{eq}$ is the overall constraints matrix and collects plastic flow constraints on discontinuities (Eq. (2)), velocity boundary conditions and external power normalization condition. n^I is the total number of internal interfaces. The reader is referred to [26] for a critical discussion of the most efficient tools (linear and non-linear) to solve Eq. (3).

6. FE simulations results

The churches have been studied numerically by means of the FE discretizations shown from Figs. 3–9. As can be noted, the meshes adopted are quite refined in order to reproduce the failure mechanisms associated with the collapse of the structures with sufficient accuracy.

From a numerical point of view, it should be noted that the quite standard discretization utilized within any commercial code to perform elastic analyses can be perfectly interfaced with the FE limit analysis code here used. This latter software requires only a plate and shell discretization by means of three-node triangular elements for masonry, with the possibility

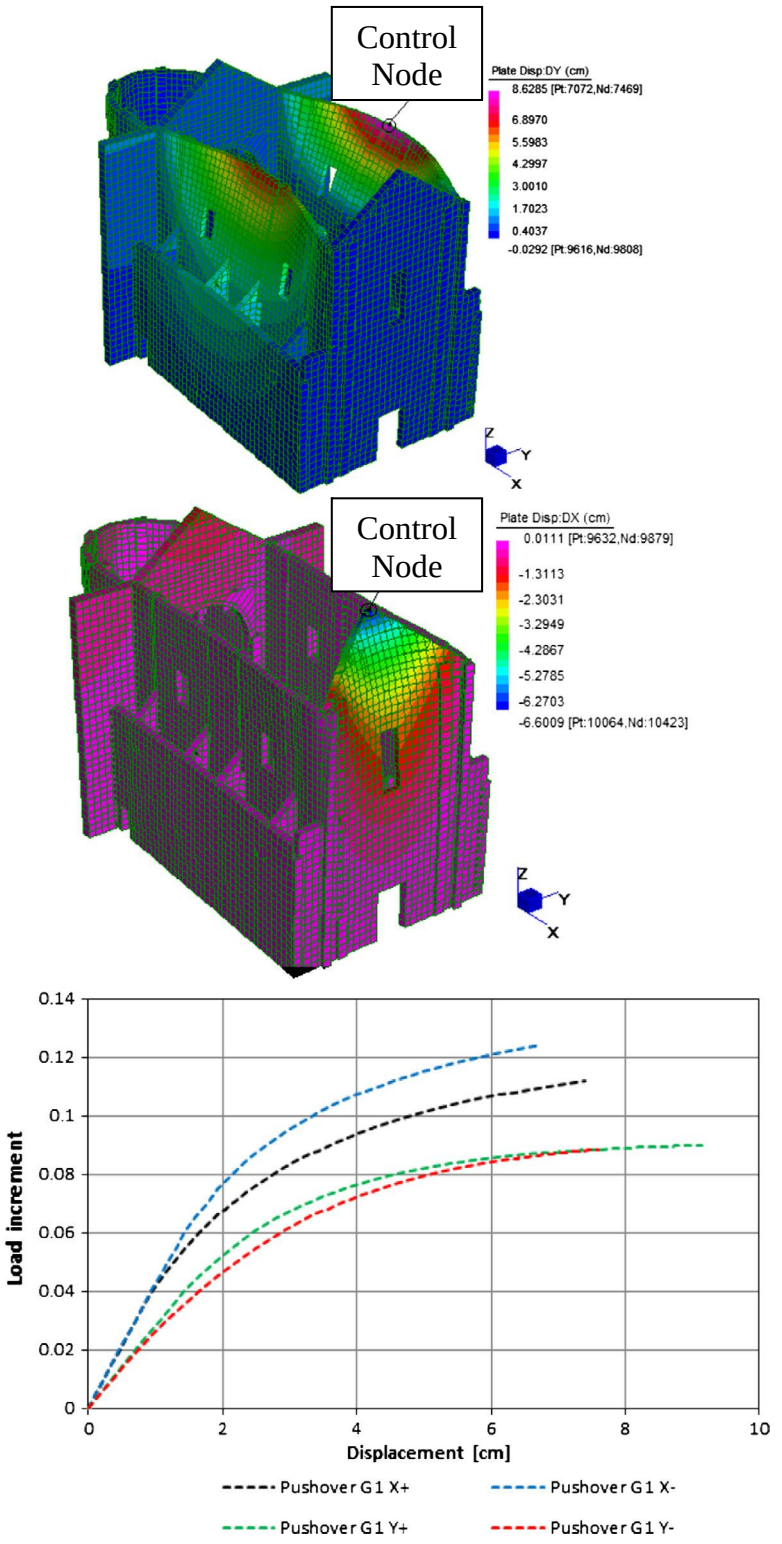

Fig. 14. Church 1, pushover G1 curves and deformed shapes at collapse for G1 distributions *Y*+ and *X*−.

of modeling mono-dimensional elements (e.g. steel and timber beams, rods or reinforced concrete ring beams) through rigid plastic trusses or beams.

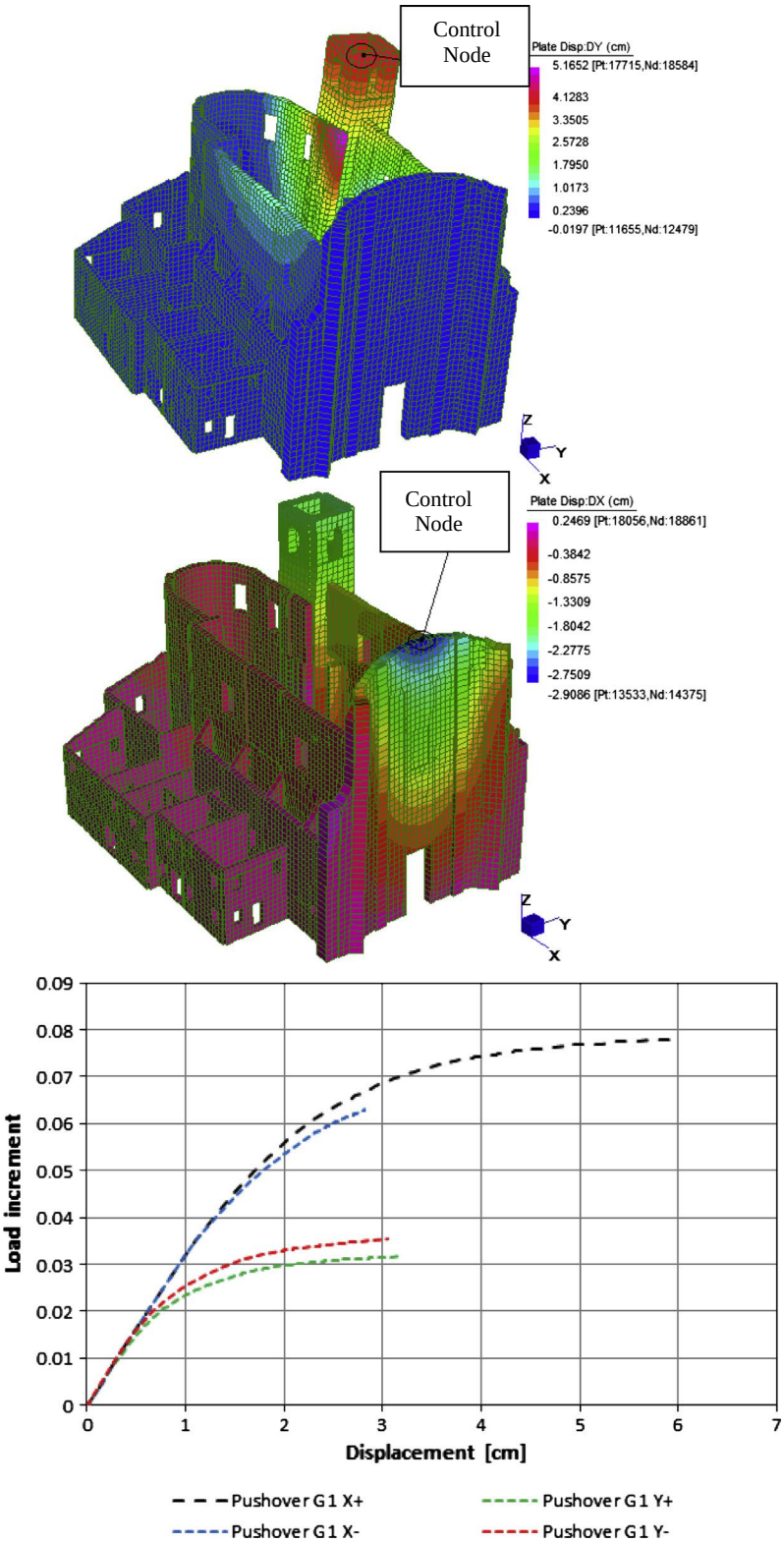

Fig. 15. Church 2, pushover G1 curves and deformed shapes at collapse for G1 distributions *Y*+ and *X*–.

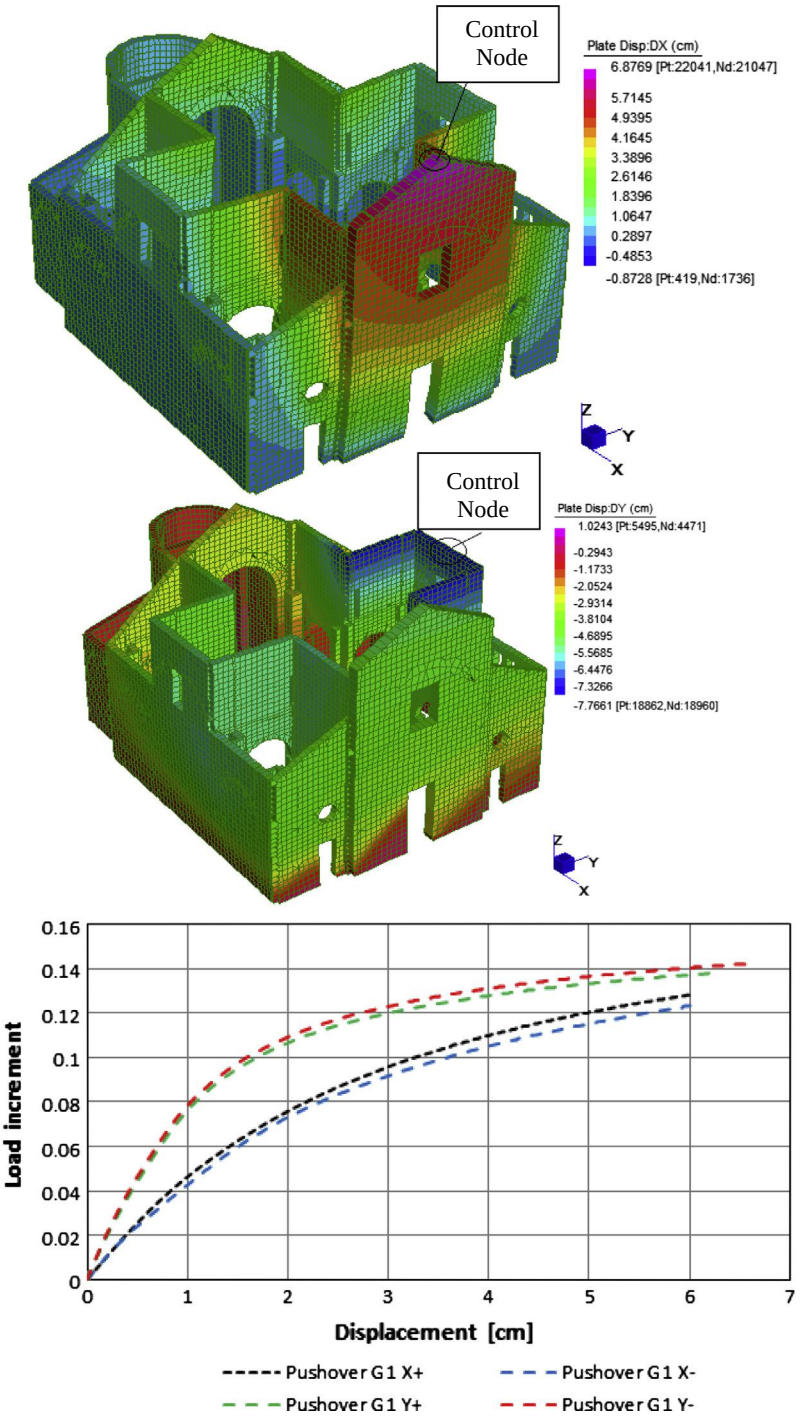

Fig. 16. Church 3, pushover G1 curves and deformed shapes at collapse for G1 distributions *X*+ and *Y*−.

6.1. FE pushover and limit analysis results

Non-linear static (pushover) analysis consists of a step-by-step procedure where horizontal loads are gradually increased, keeping gravity loads constant up to the activation of a failure mechanism in the structure.

In order to reduce the multi-DOF structure to a single-DOF system where the seismic vulnerability is assessed, Italian Code [23] requires to perform the non-linear static analysis up to a prescribed decrease of the total base shear, thus implicitly requiring the utilization of softening materials. Such approach is typically conceived for reinforced concrete frames or new

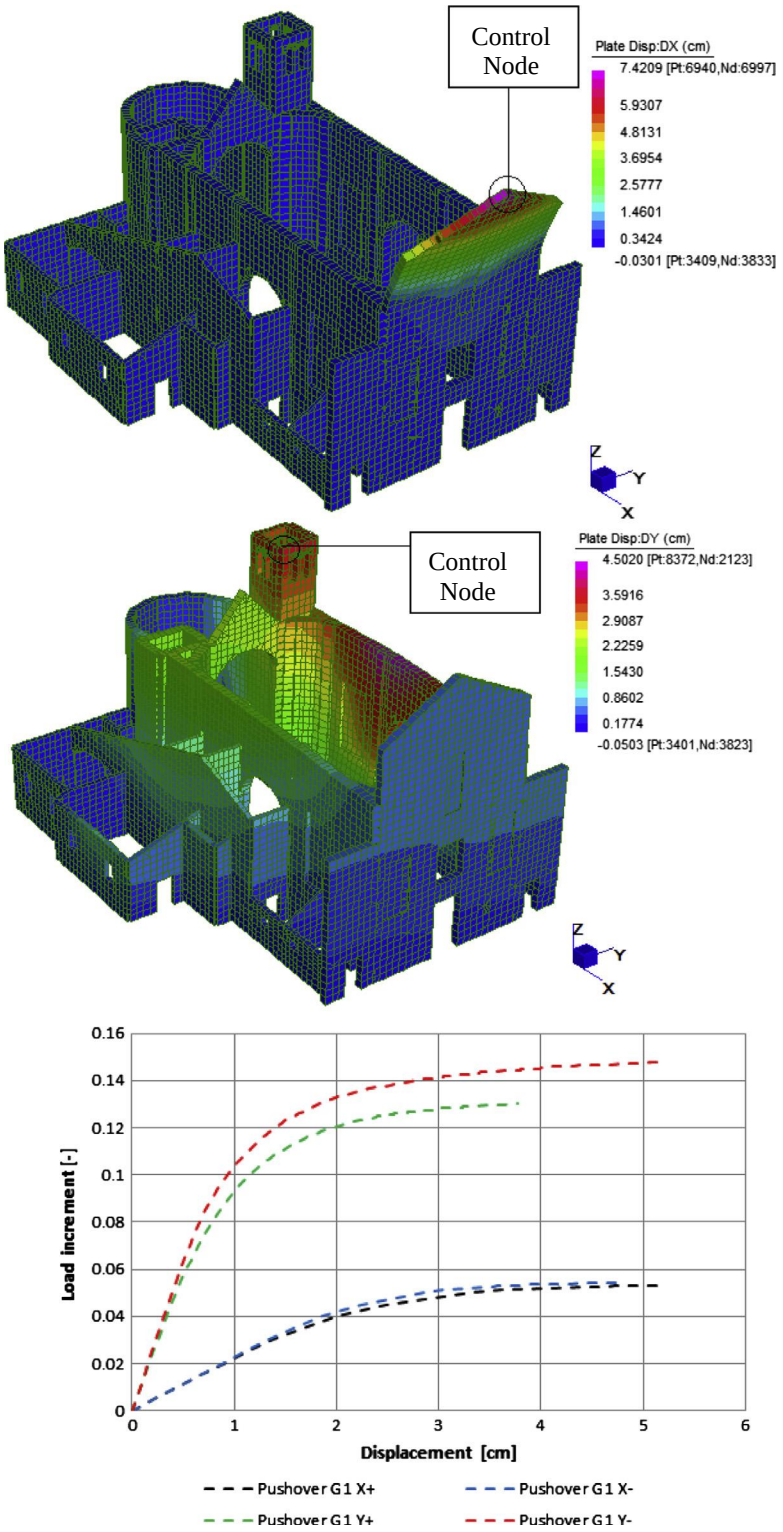

Fig. 17. Church 4, pushover G1 curves and deformed shapes at collapse for G1 distributions *X*+ and *Y*+.

masonry buildings, where the schematization with the so-called equivalent frame is admitted and to deal with softening is much easier than the general case.

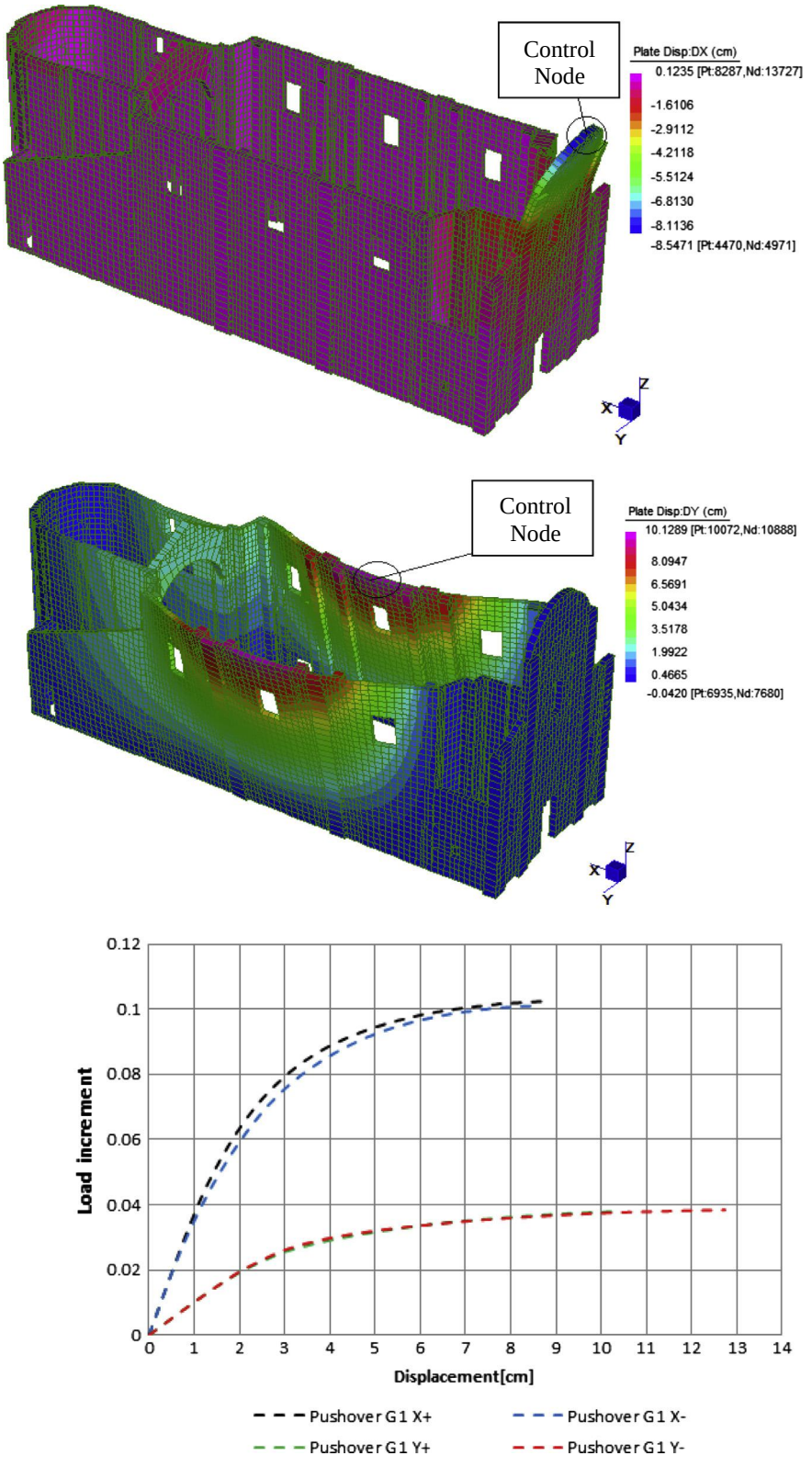

Fig. 18. Church 5, pushover G1 curves and deformed shapes at collapse for G1 distributions *X*– and *Y*+.

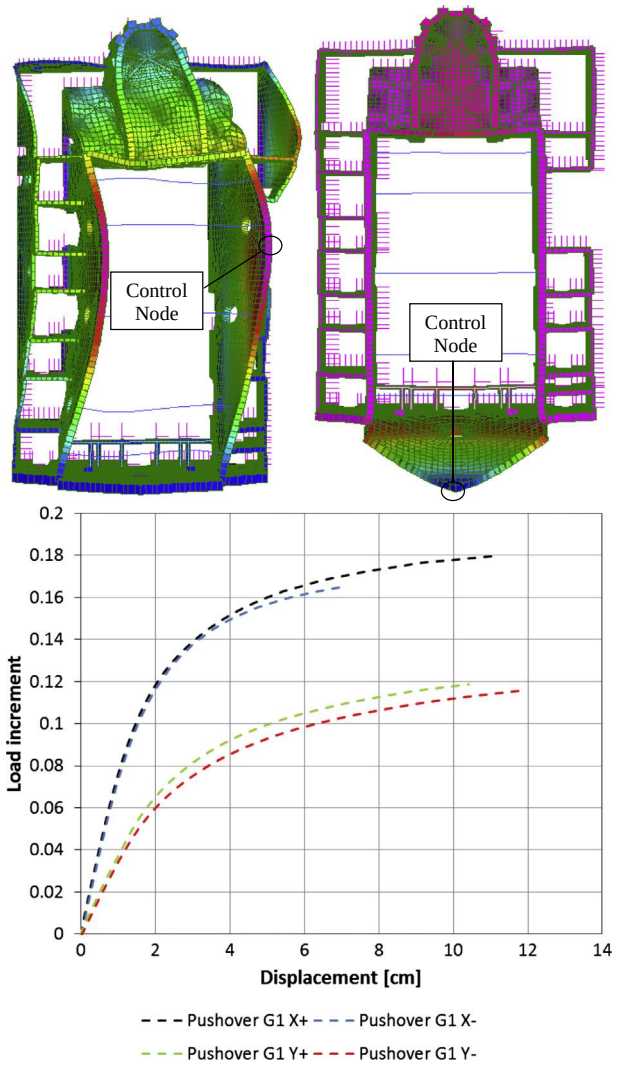

Fig. 19. Church 6, pushover G1 curves and deformed shapes at collapse for G1 distributions *X*+ and *Y*−.

Italian Guidelines for the architectural built heritage [21] allow conducting the non-linear static analysis with elastic-perfectly plastic materials, as those reported in this paper, despite the well-known inability of such models to provide a drop of the global pushover curves. It is indeed very difficult to reproduce global softening for at least two distinct reasons. The first is that rarely softening materials are at disposal in commercial codes for three- and two-dimensional finite elements (an equivalent frame approach cannot be used here for obvious reasons). The second is that, for no-tension (or scarcely resistant) materials failing out-of-plane, softening is very limited and all strength is essentially due to gravity loads.

According to Italian Code, two distributions of forces, labeled as G1 and G2, should be considered. The load case G2 is a uniform distribution of horizontal forces proportional to the mass, whereas the load case G1 is a distribution of horizontal forces proportional to the mass multiplied by the height of the element.

For each church, eight pushover analyses were repeated, one for each direction (four directions are investigated, namely longitudinal direction *X*+/− with positive and negative verse and transversal direction *Y*+/−, again with positive and negative verse) and load case (G1 and G2), iteratively choosing a control point belonging to an active failure mechanism.

It was found, as it almost always occurs for such kind of structures, that G2 load distribution is associated with a greater total base shear when compared with that provided by the corresponding G1 distribution. For this reason, hereafter, only results obtained with G1 load distributions are shown for the sake of conciseness.

According to Italian Code, in absence of softening materials, the analyses were conducted up to "meaningful displacements", without the need to define the ultimate displacement corresponding to the displacement reached in correspondence to a pre-assigned drop of the global pushover curves.

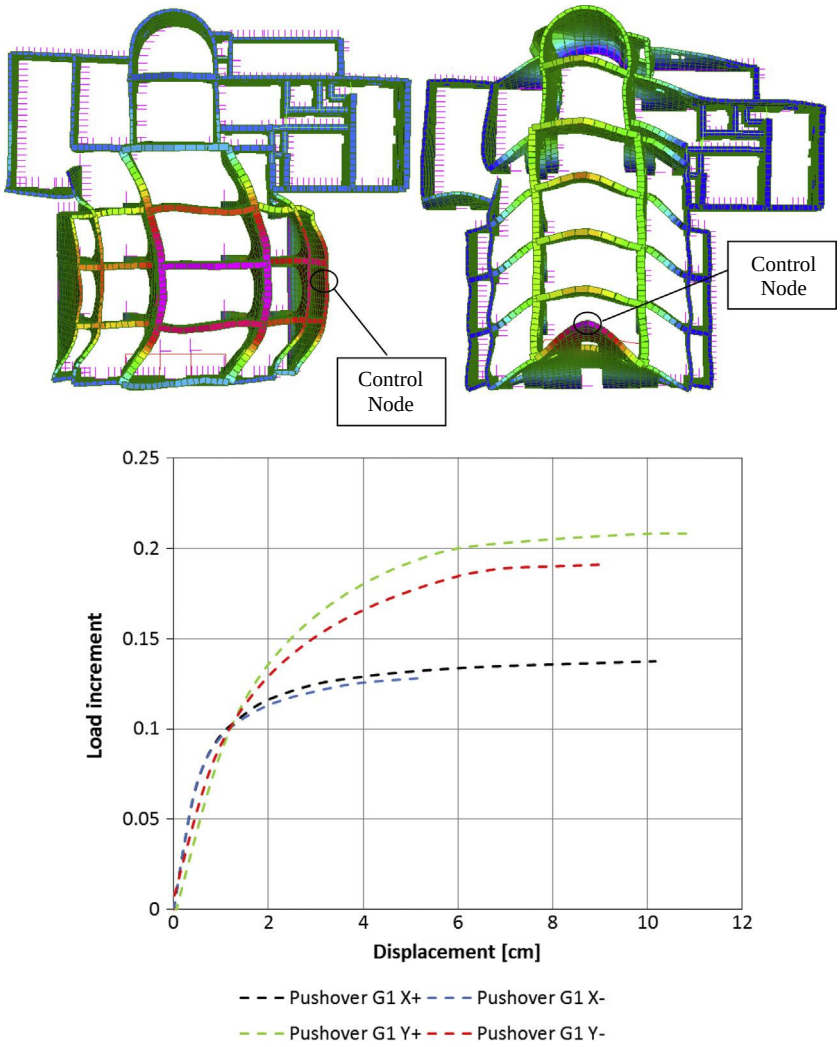

Fig. 20. Church 7, pushover G1 curves and deformed shapes at collapse for G1 distributions *X*+ and *Y*+.

Since the aim of the present paper is the evaluation of the horizontal acceleration activating a failure mechanism, it is not necessary to deepen the knowledge about the determination of meaningful displacements by the code.

Resulting pushover curves, along with the corresponding deformed shapes at peak, are summarized from Figs. 14–20.

It is worth noting that the limit multiplier indicated in the *y*-axis of each curve represents, as by explicit choice of nodal forces applied to the models, the a_g/g ratio between the horizontal acceleration associated with the activation of a failure mechanism and gravity acceleration.

As can be noted, the acceleration at collapse a_g is sometimes surprisingly low, despite the improving coefficients adopted for masonry mechanical properties within pushover analyses, already discussed in the previous section.

Deformed shapes at collapse obtained with the FE limit analysis code are again depicted from Figs. 21–27. As a rule, due to the general symmetry of the structures along their longitudinal axes, no meaningful differences are experienced between *X*+ and *X*− or *Y*+ and *Y*− directions. For this reason, here only one mechanism for *X* and *Y* directions per church is depicted for the sake of conciseness.

As can be noted, in almost all the cases, failure mechanisms are local and usually involve either the façade or the apse for the longitudinal direction and lateral walls for the transversal direction.

For a direct comparison with pushover results, deformed shapes at collapse obtained with limit analysis are reported from Figs. 21–27.

In almost all the cases, the response of limit analysis models appears in very good agreement with that found using push-over analysis. This is not surprising, because, except the lower tensile strength adopted in the limit analysis approach, which provides a lower value of the overall strength of the structure, hypotheses and discretization refinement are the same.

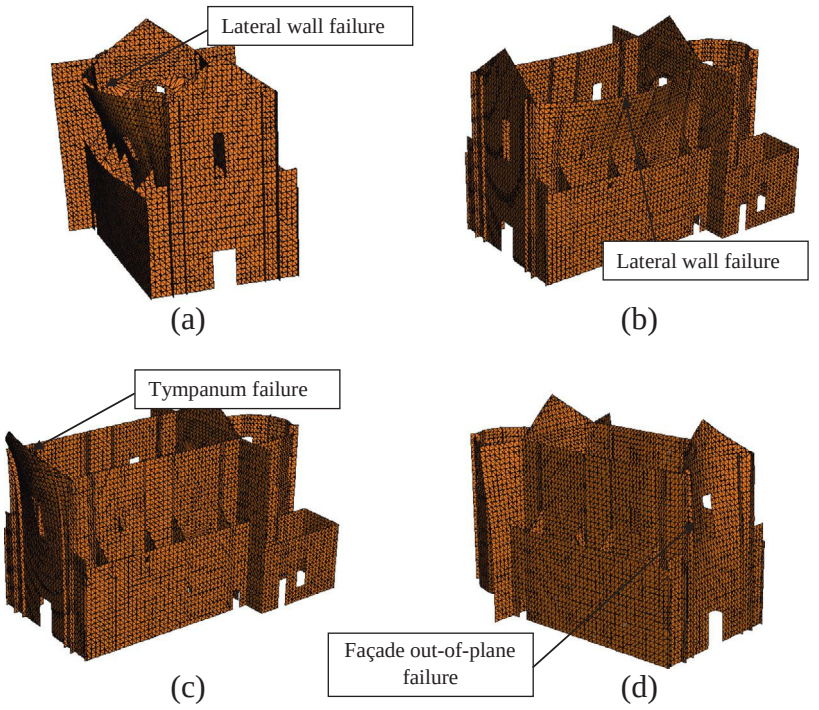

Fig. 21. Church 1. Deformed shapes at collapse obtained with FE limit analysis. (a) *Y*−. (b) *Y*+. (c) *X*+. (d) *X*−.

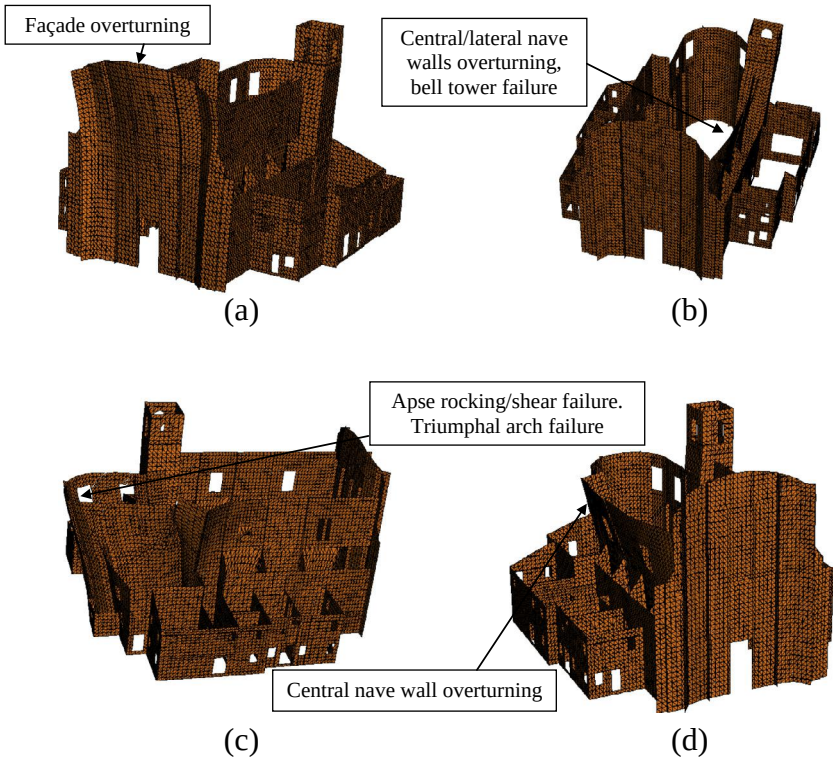

Fig. 22. Church 2. Deformed shapes at collapse obtained with FE limit analysis. (a) *X*+. (b) *Y*+. (c) *X*−. (d) *Y*−.

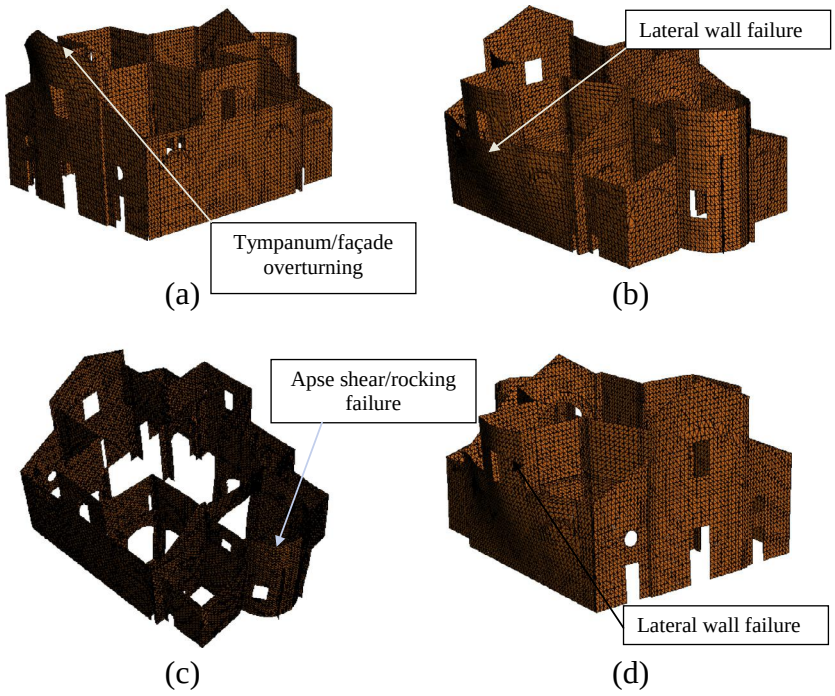

Fig. 23. Church 3. Deformed shapes at collapse obtained with FE limit analysis. (a) *X*+. (b) *Y*+. (c) *X*−. (d) *Y*−.

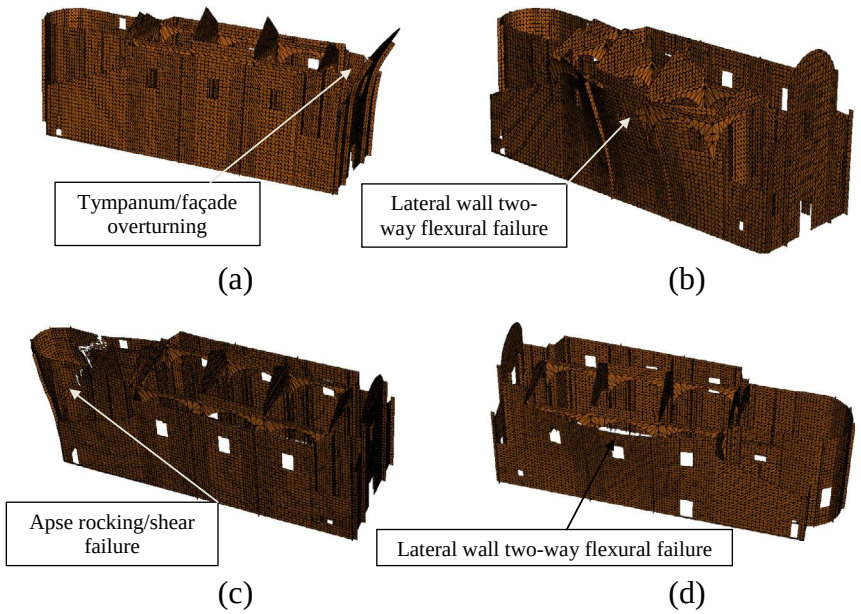

Fig. 24. Church 4. Deformed shapes at collapse obtained with FE limit analysis. (a) *X*+. (b) *Y*−. (c) *X*−. (d) *Y*+.

The advantage of limit analysis stands in the time needed to perform the simulations. As a matter of fact, a single push-over simulation may require more than one day of processing time for refined discretizations on standard PCs, whereas limit analysis is capable of providing failure mechanisms and collapse loads in less than 120 min.

7. Comparison and safety assessment

At-hand kinematic limit analyses are conducted in agreement with Italian Guidelines for the built heritage [21], consid-ering (when present) the failure mechanisms falling in the 28 different cases provided by the standard.

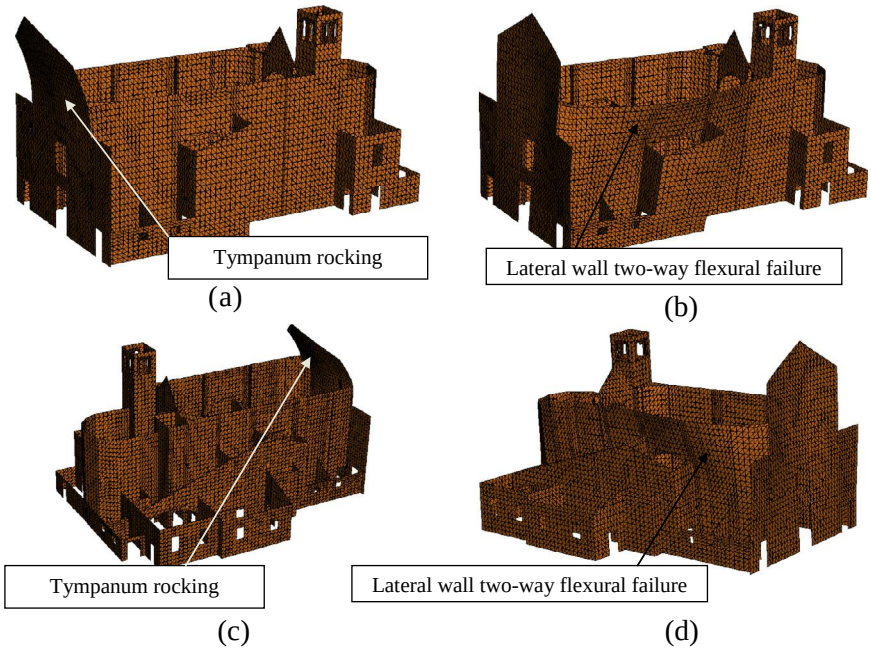

Fig. 25. Church 5. Deformed shapes at collapse obtained with FE limit analysis. (a) *X*−. (b) *Y*−. (c) *X*+. (d) *Y*+.

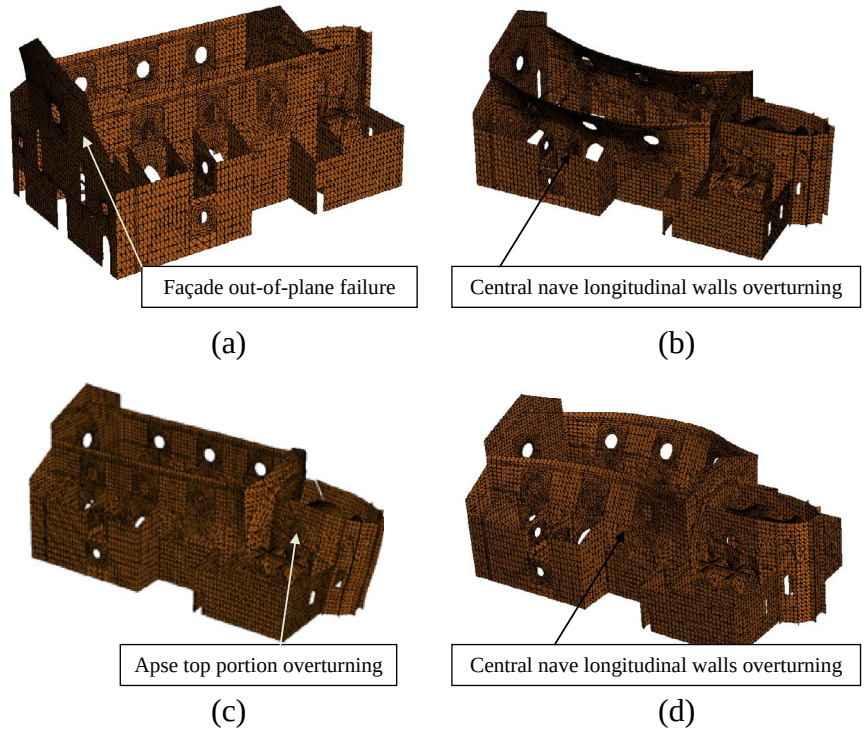

Fig. 26. Church 6. Deformed shapes at collapse obtained with FE limit analysis. (a) *Y*−. (b) *X*+. (c) *Y*+. (d) *X*−.

Masonry is assumed as an isotropic no-tension material and the acceleration at failure, when the failure mechanism is a priori-assumed, is simply evaluated by means of a CAD assisted computer program and by means of the application of the principle of virtual works under small deformations.

The resultant horizontal accelerations are summarized in bar graphs reported for each church from Figs. 28–34.

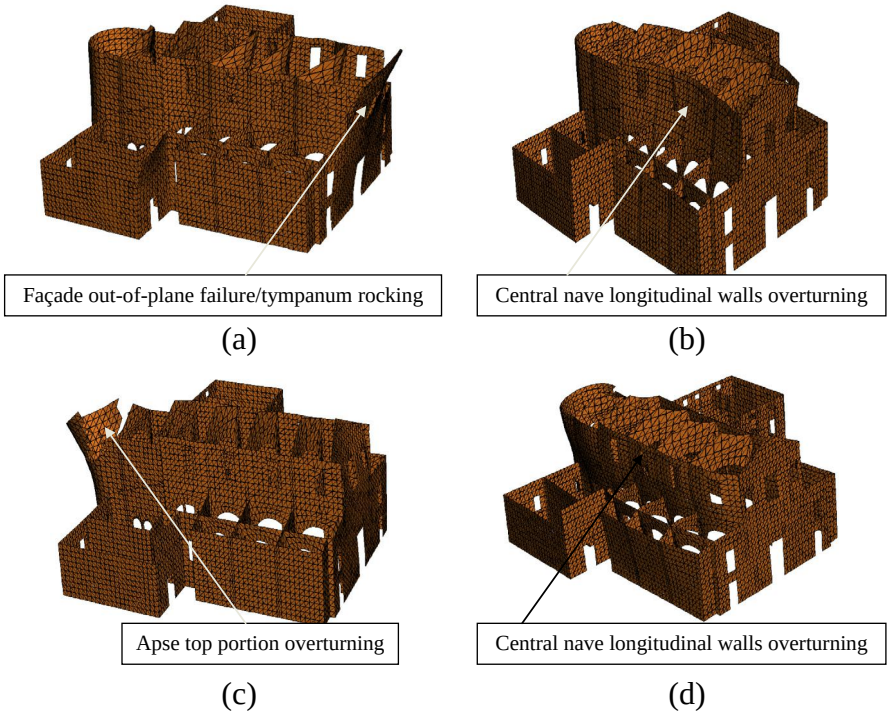

Fig. 27. Church 7. Deformed shapes at collapse obtained with FE limit analysis. (a) *Y*−. (b) *X*+. (c) *Y*+. (d) *X*−.

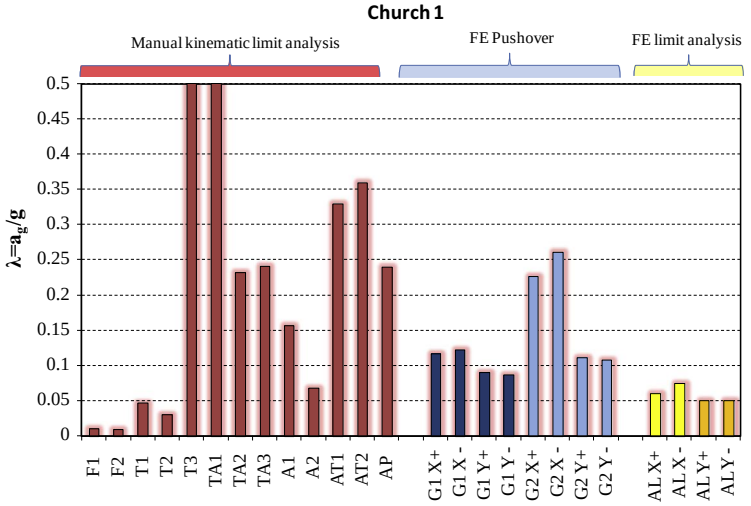

Fig. 28. Church 1. Comparison among the different failure multipliers (representing a_g/g) obtained with the different approaches. Red: limit analysis with pre-assigned failure mechanisms. Blue: pushover. Yellow: FE limit analysis. (For interpretation of the references to color in this figure legend, the reader is referred to the web version of this article.)

Red bars refer to partial failure mechanisms evaluated according to manual limit analysis. For the sake of completeness, the corresponding accelerations at failure found using FE pushover and limit analyses are also represented (blue and yellow bars, respectively). Each bar is associated with a label, describing: (1) the failure mechanism considered (for manual kinematic limit analysis); (2) the load case and direction with positive and negative verse (for FE pushover analysis); (3) the direction with positive and negative verse (for FE limit analysis).

The meaning of the labels (limiting the list to manual kinematic limit analysis) is the following:

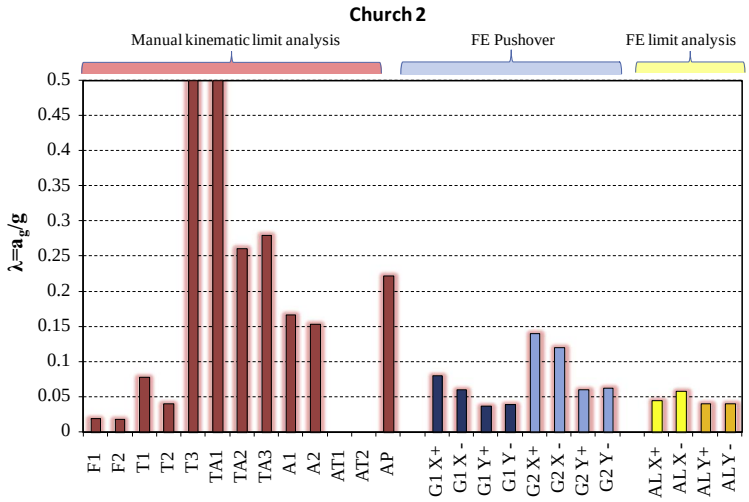

Fig. 29. Church 2. Comparison among the different failure multipliers (representing a_g/g) obtained with the different approaches. Red: limit analysis with pre-assigned failure mechanisms. Blue: pushover. Yellow: FE limit analysis. (For interpretation of the references to color in this figure legend, the reader is referred to the web version of this article.)

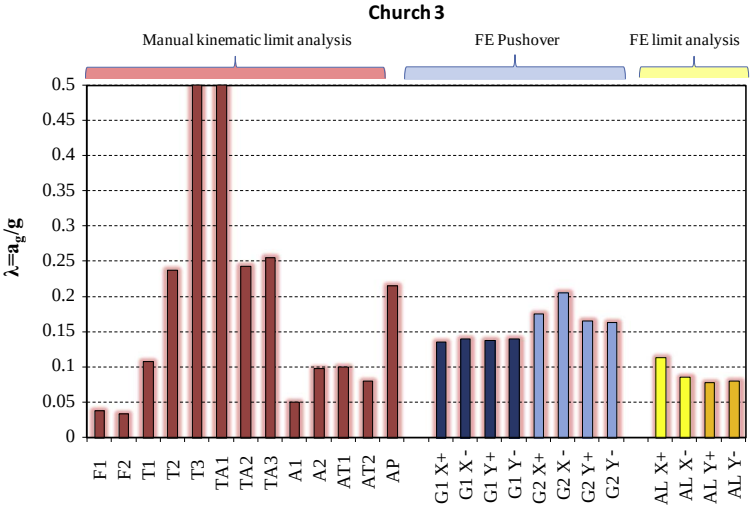

Fig. 30. Church 3. Comparison among the different failure multipliers (representing a_g/g) obtained with the different approaches. Red: limit analysis with pre-assigned failure mechanisms. Blue: pushover. Yellow: FE limit analysis. (For interpretation of the references to color in this figure legend, the reader is referred to the web version of this article.)

- F stands for façade overturning. Two collapse mechanisms are investigated, namely overturning with a horizontal yield line positioned on the base (F1) and at a middle height (F2). The conservative hypothesis of bad interlocking between façade and perpendicular walls is made, obviously resulting in very low horizontal accelerations associated with the activation of the failure mechanism.
- T stands for tympanum overturning. Three possible failures may occur; the first with horizontal hinge at the base of the tympanum, the second with horizontal hinge passing through the top of the central nave gable roof (if the tympanum is higher than the nave) and the third with inclined yield lines.
- TA refers to in-plane shear failures of the façade. TA1 is a mechanism with vertical central hinge involving the formation of two symmetric piers, TA2 involves the formation of two shear walls at the base with a horizontal crack passing through the top of the main entrance, TA3 is constituted by a diagonal crack running through the whole façade. Again, in order to obtain conservative results, the hypothesis of vanishing interlocking between façade and perpendicular walls is made.
- A is related to transversal lateral walls failure, A1 and A2 indicating an external and internal overturning, respectively.

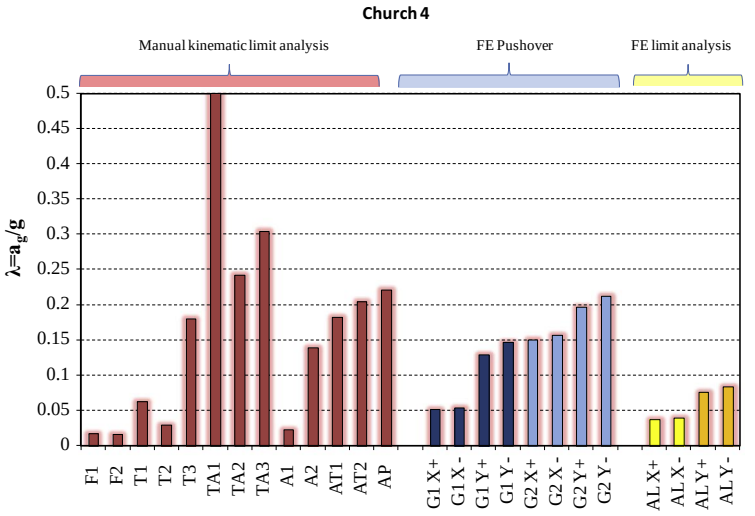

Fig. 31. Church 4. Comparison among the different failure multipliers (representing a_g/g) obtained with the different approaches. Red: limit analysis with pre-assigned failure mechanisms. Blue: pushover. Yellow: FE limit analysis. (For interpretation of the references to color in this figure legend, the reader is referred to the web version of this article.)

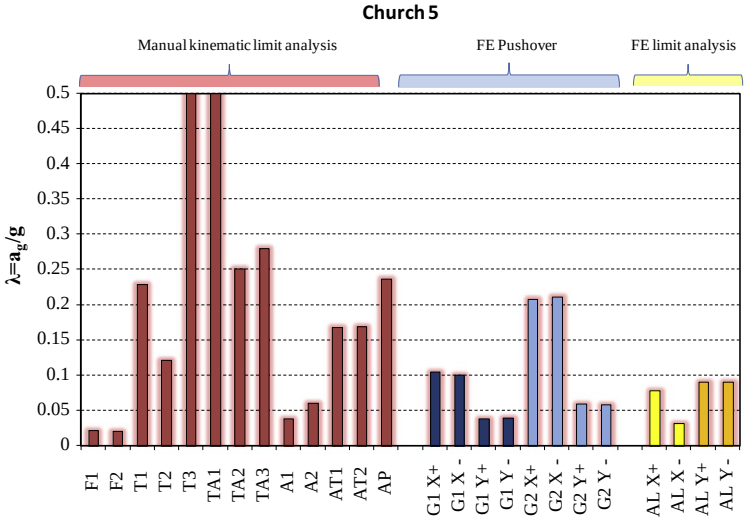

Fig. 32. Church 5. Comparison among the different failure multipliers (representing a_g/g) obtained with the different approaches. Red: limit analysis with pre-assigned failure mechanisms. Blue: pushover. Yellow: FE limit analysis. (For interpretation of the references to color in this figure legend, the reader is referred to the web version of this article.)

- AT1 and AT2 refer to the triumphal arch behavior, with the overturning of a single or both abutments, respectively.
- AP refers to the overturning of the apse.

As can be noted from a comparative analysis of the accelerations at failure and active mechanisms found by means of the three different approaches, the following general considerations may be done:

- At-hand kinematic limit analysis based on failure mechanisms is usually associated with very low accelerations at failure, especially when dealing with façade (F) and tympanum (T) overturning. This is obviously a consequence of the assumption made for the masonry constitutive behavior (no-tension material) as well as of the conservative hypothesis of bad interlocking between perpendicular walls (especially for the façade behavior).
- The accelerations at failure obtained from limit analysis are always slightly larger than those provided by pre-assigned mechanisms. In the numerical model, indeed, a small but not vanishing tensile strength is assumed for masonry.

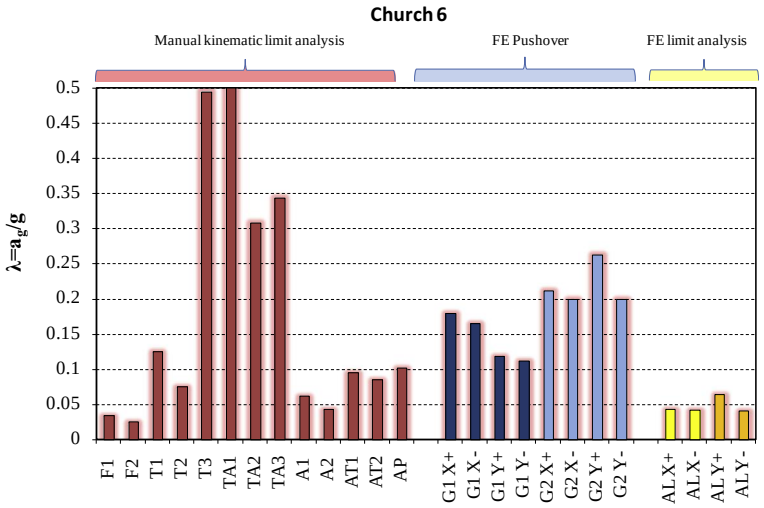

Fig. 33. Church 6. Comparison among the different failure multipliers (representing a_g/g) obtained with the different approaches. Red: limit analysis with pre-assigned failure mechanisms. Blue: pushover. Yellow: FE limit analysis. (For interpretation of the references to color in this figure legend, the reader is referred to the web version of this article.)

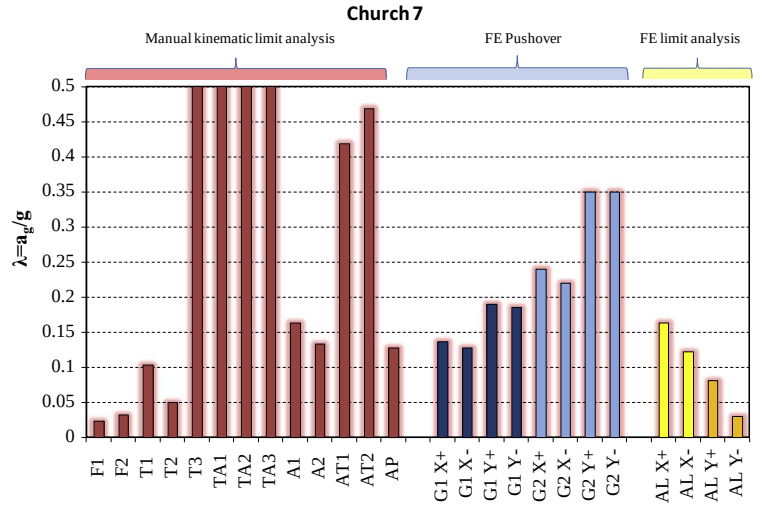

Fig. 34. Church 7. Comparison among the different failure multipliers (representing a_g/g) obtained with the different approaches. Red: limit analysis with pre-assigned failure mechanisms. Blue: pushover. Yellow: FE limit analysis. (For interpretation of the references to color in this figure legend, the reader is referred to the web version of this article.)

From a comparative detailed inspection of the failure mechanisms, the following conclusions may be drawn:

- In Church 1, when the seismic load acts longitudinally, the façade fails for the activation of an overturning mechanism. While in both pushover and FE limit analysis the good interlocking between perpendicular walls helps in the formation of inclined yield lines localized on the upper part, mainly involving the tympanum, the lower acceleration provided by manual limit analysis is associated with an overturning mechanism with horizontal hinge at the middle height (F2). On the other hand, an overturning with hinge at the base (F1) requires a very similar acceleration. When dealing with the transversal horizontal loads, failure is associated with out-of-plane failure of the lateral walls of the nave. In this case, manual kinematic limit analysis is in good agreement with results provided by both pushover and FE limit analysis. Damage surveys result in agreement with all numerical predictions, indicating damages concentrating on façade and lateral walls.
- In Church 2, again for a seismic load acting along a longitudinal direction, façade overturning occurs, as correctly predicted by all the models used. The transversal behavior is again governed by external lateral walls out-of-plane failure, but in this case partially involving the façade, which appears to suffer severe damage for in-plane shear actions.

This issue is well reproduced by both pushover and limit analysis. At-hand kinematic limit analysis, as a consequence of the simplifications adopted on the geometry, also indicates a quite low multiplier for the partial collapse of the tympanum (T2 active failure mechanism), which indeed results totally isolated, not pre-compressed and not equipped with structural devices able to prevent its overturning.

- In Church 3, collapse loads provided by at-hand kinematic limit analysis are slightly higher than those obtained in the previous cases, because of the squater geometry of the church and the slightly larger thickness of perimeter walls. When dealing with the longitudinal behavior, all the procedures here investigated agree in indicating that the façade rocking is associated with the first active failure mechanism. When the seismic load is applied transversally, FE pushover and limit analyses indicate a complex failure involving out-of-plane movements of lateral walls, chapels shear failure and in-plane shear damage of the façade. Conversely, the procedure based on pre-assigned failure mechanisms indicates a simple first mode overturning of one of the lateral walls (A1), associated with very low horizontal accelerations. Such a result is in partial agreement with both FE pushover and limit analyses and it is probably the final result of the simplifications adopted within at-hand calculations, which don't take into account the actual geometry of the church, especially at the interconnection region between lateral chapels and longitudinal lateral walls.
- Results obtained for Church 4 are very similar to those found for Church 3, but with failure mechanisms associated with lower horizontal accelerations. Again, all models agree in indicating that the most vulnerable parts of the structure are the façade (in this case, the tympanum is very high and totally isolated from the rest of the structure) and lateral walls. The very low horizontal accelerations found at failure may be partially justified by the unusual geometry of the church, which shows a quite long single nave and a particularly slender façade. At-hand kinematic limit analysis correctly indicates that the tympanum is subjected to probable overturning at very low levels of acceleration (T2 failure mechanism).
- In Church 5, which again exhibits a quite isolated and large tympanum, active failure mechanisms are again the partial overturning of the upper part of the façade and the out-of-plane failure of the lateral walls. In this case, at-hand kinematic limit analysis very well fits results obtained using finite elements, indicating as active failure mechanisms those labeled with F2 and A1 for the longitudinal and transversal direction, respectively.
- Church 6 exhibits some common features at failure already presented by several of the other churches previously studied, namely a failure of the upper part of the façade, with clear detachment from perpendicular walls, transversal rocking of the long lateral walls and apse failure (with seismic loads acting along the longitudinal positive direction) activating in both the pushover and the FE limit analysis models. In partial agreement with the aforementioned methods, at-hand failure mechanisms indicate very low failure accelerations for the activation of façade rocking (F2), lateral walls overturning (A2) and quite low accelerations associated with the out-of-plane failure of the apse.
- In Church 7, FE pushover and limit analyses indicate that the behavior of the structure is more global, because of the presence of perpendicular arches that internally interconnect isolated masonry bearing elements and reduce the overall length of the external walls. This feature is obviously not reproducible with at-hand kinematic limit analysis,

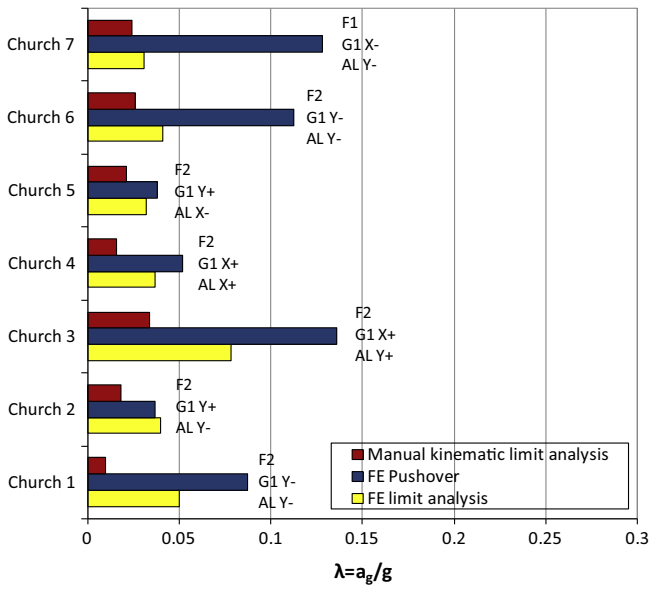

Fig. 35. Synopsis of the normalized accelerations at collapse found with the three approaches investigated (at-hand kinematic limit analysis, FE pushover, upper bound FE limit analysis).

where a very poor interlocking is hypothesized. Using this latter approach, indeed, active failure modes are again the overturning of the façade with cylindrical hinge at the base (F1), out-of-plane failure of both lateral walls (A2) and rather high vulnerability of the apse. Exception made for the more global behavior of the FE model within pushover and automatic limit analysis, again all models result in quite convincing agreement, also in light of the damages suffered by the church during the seismic sequence, see Fig. 12c.

8. Conclusions

This study has presented and discussed pros and cons of three different approaches to investigate the behavior of existing masonry churches under seismic loads. In particular, results provided by (1) at-hand kinematic limit analysis based on pre-assigned failure mechanisms (as required by Italian Guidelines on built heritage [21]), (2) global FE pushover approach and (3) FE upper bound limit analysis have been critically analyzed and compared. The different procedures have been systematically applied on seven churches that suffered damage during the recent 2012 Emilia-Romagna earthquake sequence.

The collapse accelerations estimated with the three approaches inspected are schematically reported in Fig. 35. When dealing with at-hand kinematic limit analysis, in agreement with the upper bound theorem, the failure mechanism associated to the smallest acceleration is the active one. It is generally found that façades (and in particular tympanums) exhibit an extremely high vulnerability. The reason is linked to both the geometry of the façades (slender walls) and the very poor interlocking with perpendicular walls. In agreement with at-hand limit analysis, both pushover and upper bound FE limit analyses indicate as active, in almost the totality of the cases, very similar failure mechanisms. The higher collapse accelerations found come from the non-vanishing cohesion assumed in the latter approaches and the good interlocking hypothesis. The use of either traditional (steel bars) or innovative (FRP retrofitting, smart wires with seismic dissipation) strengthening techniques is effective to inhibit façade overturning. However, an important feature of all the analyses conducted is their capability to identify all those structural elements that may activate a failure mechanism at low horizontal accelerations. As a matter of fact, it is found that the formation of mechanisms on apses, lateral walls and chapels is almost always asso-ciated with quite low acceleration values, and local interventions to preclude their failure are needed in view of a seismic upgrading of the entire structure.

Finally, the huge amount of numerical data, obtained from the examples discussed in this study, allows making some general considerations on the procedures adopted. In particular, the following key issues are worth noting:

- At-hand kinematic limit analyses conducted on pre-assigned failure mechanisms are very straightforward, but too conservative in the indication of the horizontal acceleration at failure and rather sensitive to initial hypotheses assumed, especially regarding the actual interlocking between perpendicular walls. In addition, unavoidable simplifications introduced in the real geometry of the churches, usually not reducible to pre-assigned structural schemes, tend to make the computations less near to the real case under study, thus implicitly making the accelerations found not fully predictive of the actual behavior of the structure.
- FE pushover analyses conducted by commercial codes are very demanding from a computational point of view and require technicians experienced in non-linear incremental procedures, but may provide an interesting indication of the actual failure mechanisms active on the structure under study. Again, material parameters adopted and hypotheses done on interlocking between neighboring walls, as well as an indication of the floors stiffness, are crucial for the subsequent behavior of the structure in the inelastic range. In addition, the assumption of simple material models for masonry at failure, as those available in the most diffused codes (as for instance the Mohr–Coulomb failure criterion), severely limits the application to a very preliminary identification of the most critical zones of the church. However, when such zones are assumed as critical, more sophisticated analyses on single portions are still possible to refine the estimated accelerations at collapse and actual active failure patterns.
- Finally, FE limit analysis appears the most suitable to be applied in all those cases where partial failure mechanisms are more likely (as in the case of masonry churches) and there is the need to perform refined computations, taking into account the actual geometry of the structure and assuming sophisticated material models for masonry. In particular, FE limit analysis has the great advantage of automatically providing the active failure mechanism, utilizing the same discretization used for linear FE computations.

Acknowledgements

This work has been carried out within a research agreement between Politecnico di Milano and Curia di Ferrara, under the scientific responsibility of Eng. Gabriele Milani (Politecnico) and Eng. Don Stefano Zanella (Curia), who is gratefully acknowledged by the authors.

Part of the analyses were developed within the activities of Rete dei Laboratori Universitari di Ingegneria Sismica – ReLUIS for the research program funded by the Dipartimento di Protezione Civile – Progetto Esecutivo 2014. Eng. Maurizio Acito is gratefully acknowledged for the use of a licensed version of Straus7.

References

[1] Doglioni F, Moretti A, Petrini V. Le chiese e il terremoto. Edizioni LLINT, Trieste, Italy; 1994 [Churches and earthquake].
[2] Ramos L, Lourenço PB. Modeling and vulnerability of historical city centers in seismic areas: a case study in Lisbon. Eng Struct 2004;26:1295–310.
[3] Giuffrè A, editor. Safety and conservation of historical centers: the Ortigia case. Roma – Bari: Laterza Press; 1993.
[4] Lagomarsino S, Resemini S. The assessment of damage limitation state in the seismic analysis of monumental buildings. Earthq Spect 2009;25(2):323–46.
[5] Lourenço PB, Roque JA. Simplified indexes for the seismic vulnerability of ancient masonry buildings. Constr Build Mater 2006;20:200–8.
[6] Roque JA. Strengthening and structural rehabilitation of old masonry walls/Reforço e reabilitação estrutural de paredes antigas de alvenaria. MSc thesis. Universidade do Minho; 2002 [in Portuguese].
[7] Milani G, Venturini G. Automatic fragility curve evaluation of masonry churches accounting for partial collapses by means of 3D FE homogenized limit analysis. Comput Struct 2011;89:1628–48.
[8] Milani G, Venturini G. Safety assessment of four masonry churches by a plate and shell FE non-linear approach. J Perform Constr Facil 2013;27(1):27–42.
[9] Milani G. Lesson learned after the Emilia Romagna, Italy, 20–29 May 2012 earthquakes: a limit analysis insight on three masonry churches. Eng Fail Anal 2013;34:761–78.
[10] Augusti G, Ciampoli M, Zanobi S. Bounds to the probability of collapse of monumental buildings. Struct Saf 2002;24:89–105.
[11] Augusti G, Ciampoli M, Giovenale P. Seismic vulnerability of monumental buildings. Struct Saf 2001;23:253–74.
[12] Brandonisio G. Analisi di edifici a pianta basilicale soggetti ad azioni sismiche. PhD thesis. Italy: II University of Naples; 2007 [Analysis of structures with basilica plan subjected to seismic actions].
[13] Giordano A. Sulla capacità sismica delle chiese a pianta basilicale. PhD thesis. Italy: University of Naples Federico II; 2001 [On the seismic capacity of churches with basilica plan].
[14] Devaux M. Seismic vulnerability of cultural heritage buildings in Switzerland. PhD thesis. Switzerland: EPFL Lausanne; 2008.
[15] Iervolino I, Chioccarelli E, De Luca F. Preliminary study of Emilia (May 20th 2012) earthquake ground motion records. Reluis report V2.11; 2012. <http://www.reluis.it>.
[16] Iervolino I, Chioccarelli E, De Luca F. Engineering seismic demand in the 2012 Emilia sequence: preliminary analysis and model compatibility assessment. Ann Geophys 2012;2012:55.
[17] Petti L, Lodato A. Preliminary spatial analysis and comparison between response spectra evaluated for Emilia Romagna earthquakes and elastic demand spectra according to the new seismic Italian code 2012. <http://www.reluis.it>.
[18] Beolchini G, Milano L, Antonacci E. Regione Molise (Italy). Decreto 76 03/08/ 2005. Protocollo di progettazione per la realizzazione degli interventi di ricostruzione post-sisma sugli edifici privati; 2006 [Design protocol for the realization of post-earthquake reconstruction interventions on private buildings].
[19] Lagomarsino S, Podestà S. Metodologie per l'analisi di vulnerabilità delle chiese. Atti del IX Convegno Nazionale "L'Ingegneria Sismica in Italia". Torino 20–23 Settembre 1999 [Methodologies for the vulnerability analysis of churches].
[20] Ordinanza n° 83 del 5 Dicembre 2012. Riparazione con rafforzamento locale e ripristino con miglioramento sismico degli edifici religiosi (chiese) [Rehabilitation with local strengthening and seismic upgrading of religious structures (churches)].
[21] DPCM 9/2/2011. Linee guida per la valutazione e la riduzione del rischio sismico del patrimonio culturale con riferimento alle Norme tecniche delle costruzioni di cui al decreto del Ministero delle Infrastrutture e dei trasporti del 14 gennaio 2008 [Italian guidelines for the evaluation and the reduction of the seismic risk for the built heritage, with reference to the Italian norm of constructions].
[22] STRAUS7®. Theoretical manual-theoretical background to the Strand7 finite element analysis system; 2004.
[23] DM 14/01/2008. Nuove norme tecniche per le costruzioni. Ministero delle Infrastrutture (GU n.29 04/02/2008), Rome, Italy [New technical norms on constructions].
[24] Circolare n° 617 del 2 febbraio 2009. Istruzioni per l'applicazione delle nuove norme tecniche per le costruzioni di cui al decreto ministeriale 14 gennaio 2008 [Instructions for the application of the new technical norms on constructions].
[25] Fieni C, Mantovani A. Comportamento sismico delle chiese in muratura, analisi di 5 chiese dopo il sisma del Maggio 2012 in Emilia-Romagna. MSc thesis. Italy: Technical University of Milan; 2013 [Seismic behavior of masonry churches. Analysis of 5 churches after the Emilia-Romagna, May 2012, earthquake].
[26] Milani G, Lourenço PB, Tralli A. Homogenised limit analysis of masonry walls. Part II: structural examples. Comput Struct 2006;84:181–95.
[27] Milani G, Lourenço PB, Tralli A. Homogenised limit analysis of masonry walls. Part I: failure surfaces. Comput Struct 2006;84:166–80.
[28] Milani G, Lourenço PB, Tralli A. A homogenization approach for the limit analysis of out-of-plane loaded masonry walls. J Struct Eng ASCE 2006;132(10):1650–63.
[29] Milani G, Lourenco PB, Tralli A. 3D homogenized limit analysis of masonry buildings under horizontal loads. Eng Struct 2007;29(11):3134–48.
[30] Cecchi A, Milani G, Tralli A. A Reissner-Mindlin limit analysis model for out-of-plane loaded running bond masonry walls. Int J Solids Struct 2007;44(5):1438–60.
[31] Zuccarello FA, Milani G, Olivito RS, Tralli A. A numerical and experimental analysis of unbonded brickwork panels laterally loaded. Constr Build Mater 2009;23(5):2093–106.